Alma Mater Studiorum · Università di Bologna

DOTTORATO DI RICERCA IN

SALUTE, SICUREZZA E SISTEMI DEL VERDE

Ciclo XXXVI

Settore Concorsuale: 07/C1

Settore Scientifico Disciplinare: AGR/10

Computational Fluid Dynamics Applied to Indoor and Outdoor Environments for Green and Smart Production Processes

SUPERVISORE:

Dott. Marco Bovo

CO-SUPERVISORE:

Prof.ssa Beatrice Pulvirenti

Prof.ssa Stefania Toselli

PRESENTATO DA:

Shahad Hasan Flayyih Al-Rikabi

COORDINATORE DOTTORATO:

Prof.ssa Patrizia Tassinari

Esame finale anno 2024

Abstract

This thesis presents a deep investigation into the application of Computational Fluid Dynamics (CFD) for enhancing green and smart production processes in different environmental conditions. Through three related studies, the research demonstrates the flexibility of CFD in optimizing microclimate management for both indoor agricultural conditions and outdoor urban landscapes, contributing significantly to the fields of environmental management, urban planning, and agricultural sciences.

The first part of the research investigates the critical area of greenhouse microclimate control, a key factor in maximizing crop growth and productivity. This study begins with a detailed experimental analysis within a naturally ventilated greenhouse cultivating sweet pepper plants, focusing on the spatial distribution of temperature and air velocity. This model employs a porous media approach to simulate the presence and effects of crops, following Darcy's law. It integrates considerations of energy balance, including both mass transfer and heat exchange under varying climatic conditions. The resulting simulations provide an understanding of the complex thermal interactions between crops, indoor air, and soil. This innovative approach marks a significant advancement in accurately modeling and assessing greenhouse microclimates, offering crucial information for optimizing

indoor agricultural environments.

In the second study, the focus shifts to the aerodynamic properties of specific crops, particularly Basil and Mentuccia, and how their structural characteristics influence aerodynamic forces such as drag. Using advanced image processing methods, this research accurately quantifies the Leaf Area Density (LAD) of these crops. These measurements allow for a precise differentiation between the leafy areas and the porous spaces within the crops, which is crucial for an accurate aerodynamic analysis. The study highlights a strong association between the plants' morphological features, canopy density, and their aerodynamic drag coefficients across varying wind speeds. These findings are important in improving crop behavior modeling within CFD simulations. Moreover, this knowledge extends beyond theoretical aerodynamics, offering practical applications in agricultural planning and design, enhancing crop arrangement for improved efficiency, and developing a deeper understanding of plant-environment interactions.

The third and final study expands the application of CFD to an outdoor urban context, investigating the role of trees and water bodies in influencing wind patterns and temperature regulation in an urban park in Igualada, Barcelona. This part of the research integrates a porous media model with a water–air interface exchange model in three dimensional simulations. The models indicate a significant temperature reduction at pedestrian levels due to the presence of water surfaces, with the cooling effect of evaporating processes increasing significantly in downwind directions. By simulating two different scenarios, one represents both trees and a water body and the other exclusively focusing on trees. The study provides a comprehensive comparative analysis of their individual and combined cooling effects. These results highlight the impact of integrated green systems in urban

areas, emphasizing their importance in combating urban heat islands and enhancing the thermal comfort of urban residents.

Overall, this thesis not only presents the application of CFD in different environmental conditions but also indicates its potential as a powerful tool in guiding sustainable development initiatives. The research outcomes have broad implications, ranging from improving indoor agricultural production methods to informing urban green infrastructure planning, all contributing towards a more sustainable and environmentally friendly future.

Keywords: Computational Fluid Dynamics, Porous Media, Wind Tunnel, Plant Morphology, Drag Coefficient, Cooling Effect.

Contents

List of Tables

List of Figures

Chapter 1

State of Art

Computational Fluid Dynamics, as a numerical methodology for simulating fluid flow and heat transfer, has become a fundamental tool in optimizing industrial processes. Its precision and versatility make it important for industries aspiring to balance efficiency with environmental sustainability.

Within indoor environments, the application of CFD is essential for optimizing fluid dynamics, heat distribution, and mass transport. This analytical tool facilitates a comprehensive analysis of airflow patterns and temperature variations, enabling industries to create environments supportive to both productivity and environmental responsibility. For instance, in controlled indoor farming scenarios such as greenhouses, this method facilitates analyzing the optimal microclimate parameters, ensuring that crops receive the necessary conditions for growth while minimizing energy consumption.

The scope of this analytical approach extends beyond confined spaces to outdoor environments, where its impact remains innovative. In the area of urban planning, CFD is

applied in designing sustainable landscapes, optimizing wind flow, and minimizing air pollution. Specifically addressing the challenges posed by urban heat, it serves as a reliable analytical tool for assessing thermal comfort in populated areas. Through analyzing fluid dynamics and thermal patterns, it assists in strategically placing green spaces and trees, utilizing mathematical models to optimize their locations for maximum cooling impact. This systematic approach not only mitigates the adverse effects of urban heat islands but also contributes to the establishment of a comfortable and livable urban environment.

1.1 Background and motivation

Computational Fluid Dynamics in literature

The application of Computational Fluid Dynamics (CFD) in greenhouse research has undergone significant evolution since its initial use in the late 20th century. Early studies, such as those by (Okushima *et al.*, 1989), primarily focused on ventilation and design optimization of greenhouses. These informative researches laid the foundation for the application of CFD in agricultural contexts, emphasizing the importance of environmental control in greenhouse management.

However, a crucial limitation of these early models was their lack of consideration for the dynamic role of crops within the greenhouse environment. Subsequent research began to fill this gap. Notably, (Haxaire, 1999) and (Boulard *et al.*, 2002) made significant strides in modeling the distributed climate within greenhouses, particularly at the crop level. This shift marked an important progression in greenhouse CFD studies, moving from a macroscopic view of greenhouse environments to a more detailed understanding

that included the interaction between crop dynamics and environmental factors.

Further advancements were made as studies like those by (Fatnassi *et al.*, 2003, 2006, 2015), (Majdoubi *et al.*, 2009), (Kichah *et al.*, 2012), and (Tamimi *et al.*, 2013) continued to refine and expand these models. The approach of simulating the canopy as a "porous medium" became a prominent method in physical transfer modeling within crop covers. However, this phenomenological approach was not the only method used in plant modeling. Alternative approaches attempted to account for the forms of leaves and plants, and also to the level of stomata. For instance, (Roy *et al.*, 2008) combined an energy balance model with the Fluent CFD code to compute temperature and humidity at the surface of single bean leaves under low light conditions. (Defraeye *et al.*, 2014) introduced an innovative 3D CFD model that studied the convective mass transfer from leaves. This approach was unique as it merged different scales, from individual stomata to the leaf level by one comprehensive computational model. More recently, a study by (Yu *et al.*, 2022) took a closer look at how natural light and ventilation affect the climate around the plant in the greenhouse. This evolution in modeling was paralleled by technological advancements in CFD software and computational power, enabling more complex and accurate simulations. The inclusion of crop dynamics in CFD models allowed for a more accurate representation of the microclimates within greenhouses, accounting for the critical impact of crops on airflow, temperature distribution, and humidity levels.

Climate Change and Its Impact on Agriculture

The need for better greenhouse models has become increasingly critical due to the challenges of climate change. Agriculture, heavily reliant on stable climatic conditions, is now

facing threats as our global climate undergoes dramatic shifts. These changes manifest as unpredictable and extreme weather patterns, including more frequent and intense storms, erratic temperature fluctuations, and a growing trend of both droughts and floods. Such conditions stand as a direct threat to agricultural stability and productivity.

In an effort to combat these challenges, a significant focus has been placed on enhancing greenhouse technologies. The goal is to develop greenhouses that can sustain ideal growing environments for crops while minimizing the need for high energy inputs. A key strategy in this effort is the implementation of natural ventilation systems. These systems aim to lessen the dependency on energy-heavy mechanical systems, such as fans and thermal heater units. The main objective is to design greenhouses that are not just energy-efficient, but also capable of withstanding and adapting to the unpredictable and often harsh conditions brought about by a changing climate.

Urban Planning and the Role of Green and Blue Spaces

Climate change's effects aren't confined to agricultural infrastructures; they significantly impact urban environments as well. Cities, with their dense concentrations of concrete and asphalt, become hot spots for the urban heat island effect. These materials, known for their heat-absorbing properties, exacerbate the warming trends already in play due to climate change. This not only raises urban temperatures but also brings about significant health and comfort issues for city residents.

In response to these urban challenges, the importance of integrating green and blue spaces, like parks, gardens, ponds, and lakes, into city planning has been increasingly recognized. These natural spaces serve purposes more than just aesthetic enhancement

and activity area in urban settings. By offering shade and facilitating evapotranspiration, they significantly reduce local temperatures, thereby fostering urban environments that are not only more pleasant but also healthier for their inhabitants.

Linking CFD, Agriculture, and Urban Environment

This thesis contributes to the understanding of the complex relationship between indoor environments like greenhouses and the outdoor environment, using Computational Fluid Dynamics (CFD) as a key tool. It stands at the intersection of these critical areas, as it contributes to both agricultural sustainability and urban climate resilience.This approach aligns with the comprehensive goals of sustainable development, aiming to enhance crop production efficiency through clean, renewable methods while also improving urban living conditions in the face of escalating climate challenges.

1.1.1 Governing equations

The fundamental equations for solving flow physics include the Conservation of Mass (continuity equation), Conservation of Momentum (Newton's second law), and Conservation of Energy (first law of thermodynamics), which are mathematically expressed in the Navier-Stokes equations. These equations describe the motion of fluid substances, such as water and air, considering their macroscopic properties like velocity, pressure, density, and temperature.

Continuity equation express the conservation of mass and represented as

$$\frac{\partial \rho}{\partial t} + \nabla \cdot (\rho\, u) = 0 \tag{1.1}$$

where, ρ is the fluid density (kgm^{-3}), t is time (s), and u is the velocity vector (ms^{-1}). Momentum equations in the x, y, and z directions, respectively, are:

$$\rho\left(u_x\frac{\partial u_x}{\partial x}+u_y\frac{\partial u_x}{\partial y}+u_z\frac{\partial u_x}{\partial z}\right)=-\frac{\partial p}{\partial x}+(\mu+\mu_t)\left(\frac{\partial^2 u_x}{\partial x^2}+\frac{\partial^2 u_x}{\partial y^2}+\frac{\partial^2 u_x}{\partial z^2}\right) \tag{1.2}$$

$$\rho\left(u_x\frac{\partial u_y}{\partial x}+u_y\frac{\partial u_y}{\partial y}+u_z\frac{\partial u_y}{\partial z}\right)=-\frac{\partial p}{\partial y}+(\mu+\mu_t)\left(\frac{\partial^2 u_y}{\partial x^2}+\frac{\partial^2 u_y}{\partial y^2}+\frac{\partial^2 u_y}{\partial z^2}\right) \tag{1.3}$$

$$\rho\left(u_x\frac{\partial u_z}{\partial x}+u_y\frac{\partial u_z}{\partial y}+u_z\frac{\partial u_z}{\partial z}\right)=-\frac{\partial p}{\partial z}+(\mu+\mu_t)\left(\frac{\partial^2 u_z}{\partial x^2}+\frac{\partial^2 u_z}{\partial y^2}+\frac{\partial^2 u_z}{\partial z^2}\right) \tag{1.4}$$

where, ρ is the fluid density, u_x, u_y and u_z are the velocity components in the x, y, and z directions, p is the pressure, μ is the viscosity, and μ_t is the turbulent viscosity, a function of the turbulence kinetic energy k and its dissipation rate ϵ.

CFD tools like STAR CCM+ software, employs the Finite Volume Method (FVM) to numerically solve these governing equations. FVM is particularly effective as it divides the domain into discrete control volumes and applies the conservation laws to each volume. This method is recognized for its robustness in solving complex fluid flow problems in commercial CFD software.

1.1.2 Turbulence Model

Turbulence modeling is a critical aspect of CFD because most natural flows are turbulent. Turbulent flows exhibit fluctuations in the velocity field, which mix and cause fluctuations in transported quantities like momentum and energy. These fluctuations, often of a very small scale, can significantly increase computational expenses for engineering calculations. To address this, turbulence phenomena are commonly modeled using the Navier-Stokes equations, with turbulence models applied to solve additional unknown variables that arise from time-averaging the instantaneous governing equations.

There are different turbulent models available for CFD simulations, each one has its own strength and limitations. The Standard k-ϵ model has been widely used for its ability to balance accuracy and computational expense effectively in various flow conditions. It calculates turbulent kinetic energy, k, and dissipation rate, ϵ, using transport equations.

This equation represents the balance of turbulent kinetic energy in the flow, considering its production, transport, and dissipation. This equation captures the rate at which the turbulent kinetic energy is dissipated into thermal energy.

However, the model has limitations, especially in flows with strong adverse pressure gradients, near-wall treatments, and flows with significant curvature or rotation. To address these, variations of the k-epsilon model, such as the RNG k-epsilon and the Realizable k-epsilon models, have been developed.

1.1.3 Porous media

Porous media, as described in general terms, refers to a material consisting of a solid matrix with an interconnected void (Nield and Bejan, 1999). A porous medium is essentially

a solid body containing random pores or voids, ranging from tiny molecular interstices to larger voids.

Regarding CFD simulation, a porous media model is employed to simplify the complexity of the flow field. This model does not resolve the flow at every microscopic point. Instead, it determines an equivalent spatially-averaged flow field. To account for the effects of porous media on the macroscopic flow, such as pressure drop and turbulence intensity, momentum loss terms are added to the Navier-Stokes equations and the turbulence model equations.

When applying porous media models to specific problems, such as vegetation studies, a cell zone within the simulation must be defined where this model will be applied. However, the porous media model is fundamentally an added momentum source in the governing momentum equations. The source term consists of two parts: a viscous loss term and an inertial loss term.

Describing the exact geometry of plants in a greenhouse is a complex task that requires significant computational resources and time. As a compromise, plant rows are often considered as a porous medium. Although providing a detailed description of each plant would be ideal, assimilating the canopy to a porous medium is a practical and efficient method to understand and simulate the influence of vegetation on airflow within an environment.

1.1.3.1 Darcy's Law

Darcy's law states that the pressure gradient in a porous medium is proportional to the fluid's velocity, where this direct relationship reflects the fluid's viscosity and the perme-

ability of the porous medium. Darcy's law is expressed as:

$$\nabla p = -\frac{\mu}{K} u \tag{1.5}$$

where, μ represents the dynamic viscosity of the fluid, K represents the permeability of the porous medium, and u and ρ are the volume-averaged velocity and pressure, respectively.

1.1.3.2 Darcy-Forchheimer Law

Forchheimer in 1901, re-examined Darcy's experiments under conditions of higher flow rates. He noticed that at these increased rates, inertial forces significantly influenced fluid behavior, leading to a quadratic relationship between pressure gradient and velocity. In order to address these observations, Forchheimer introduced a second term to Darcy's law, to account for these inertial effects. This modified equation became:

$$\nabla p = -\frac{\mu}{K} u - \beta \rho |u| u \tag{1.6}$$

Where β is the dimensionless Forchheimer constant, $\beta = \frac{C_F}{K}$ represents the inertial coefficient.

In the agricultural fields, Darcy-Forchheimer model is particularly used in modeling the flow in crop rows. Using modern computational tools like Star CCM+ software, crop rows are effectively simulated as porous media. The momentum sink caused by the drag effect of the crop is simulated in the model, where the airflow within the crop cover, leaf area density (LAD), and drag coefficient are key parameters.

The pressure drop due to this drag effect is expressed by Darcy-Forchheimer equation, considering both viscous and inertial forces.

1.2 Thesis overview

This three-paper thesis is structured of five main chapters, each briefly outlined below.
Following this introduction (Chapter 1), Chapter 2 addresses the fundamental aspect of creating an optimal thermal environment for crops within the confines of naturally ventilated greenhouses. Employing the principles of fluid dynamics and heat transfer, this Chapter aims to establish a comprehensive framework for defining and quantifying thermal comfort parameters that are essential for sustaining crop health and maximizing yield in greenhouse conditions.
Chapter 3 shifts focus to the aerodynamic characteristics governing the interaction between crops and the surrounding airflow. By employing wind tunnel measurements and Navier-Stokes equations, this Chapter seeks to define the aerodynamic properties of horticultural crops. Understanding these properties is crucial for optimizing ventilation strategies within greenhouses, and to provide crucial empirical data for the subsequent CFD model.
Chapter 4 analyzes the effect of combining vegetation and a water body in an outdoor environment through the application of CFD, focusing on the temperature distribution and thermal comfort to assess the cooling effect of this integrated system.
Finally, Chapter 5 will represent the main conclusion founded in this work.

Chapter 2

Definition of thermal comfort of crops within naturally ventilated greenhouses

2.1 Introduction

Crop production through greenhouses has been considered the best approach to increase the growth and the development of plants by creating the right microclimate for the crops (Ghoulem *et al.*, 2019). Microclimate parameters inside the greenhouse are very critical to ensure the crop growth and controlling these parameters will result in avoiding problems such as high air temperature which is common during summer seasons (Gruda *et al.*, 2019). Therefore, the airflow pattern and thermal behavior of the greenhouse are considered the most important design features in order to keep crop transpiration and photosynthesis at acceptable levels. Natural ventilation is a cost-effective approach of controlling the microclimate parameters inside the greenhouse, it provides the transportation of mass

and heat between indoor climate conditions and the external environment while saving energy (Santolini *et al.*, 2018). Adopting the natural ventilation in the greenhouse design can facilitate the control of the microclimate parameters such as air temperature, air humidity and CO_2 concentration (Limtrakarn *et al.*, 2012). Therefore, natural ventilation is considered to be one of the most important production factors because it affects climatic control and crop quality along the year (Molina-Aiz *et al.*, 2004). The application of computational fluid dynamics (CFD) technology in the agriculture field has mainly focused on greenhouse microclimate simulation. CFD has become the key method for studying space-time phenomena in agriculture. It combines physics, chemistry, and biology to replicate complex processes. Significant progress has been made in various applications, including biological systems and agricultural buildings. (Bournet and Rojano, 2022). The use of CFD allows to simulate realistic scenarios through the application of the three conservation equations of fluid: mass, momentum, and energy, and combines the fluid turbulence model to simulate and predict the airflow pattern and the spatial distribution of factors such as temperature and humidity in the greenhouse (Bartzanas *et al.*, 2013). CFD tools can also provide the possibility to add resource terms through the user-defined function (UDF) to represent the interaction of the crop with the surrounding environment (Bekraoui *et al.*, 2022). 3D simulations in a multi-span greenhouse with an active crop have been recently developed, analyzing temperature distribution, crop transpiration model and numerical radiation model (Boulard *et al.*, 2017). Heat transfer in the greenhouse is composed of three contributions: convection, conduction and radiation. Convection is a process of heat transfer through a fluid medium that occurs due to the combined effects of buoyancy and thermal expansion. In this process, warmer and less dense air rises while cooler and denser

air descends, creating a circulation pattern. This circulation can be driven by a variety of sources such as differences in temperature between solid surfaces of walls, the ground, the crops and the air (Roy *et al.*, 2002). Conduction in greenhouses is the process by which thermal energy is transferred from one part of the greenhouse structure to another, such as from the air to the soil or from the soil to the air (Maslak, 2015). This process occurs due to the property of thermal conductivity, which is the capacity of a material to transfer heat from one region to another (Burger *et al.*, 2016). The distribution of solar radiation in greenhouses has a significant impact on crop transpiration and photosynthesis. It is highly dependent on greenhouse design, structure materials, covering materials, and weather conditions (Wang and Boulard, 2000; Santolini *et al.*, 2019). More recently, (Santolini *et al.*, 2022) studied the shading screen effect on the microclimate inside of the greenhouse, through studying the possibility to control the solar radiation that passes into the greenhouse by three different shading screens to reduce the thermal gain and to reach a thermal comfort by coupling solar radiation model with the shading screens mode. Maintaining thermal comfort in greenhouses is crucial for optimizing crop growth and productivity, with key indicators being temperature, humidity, and solar radiation, as these factors directly influence plant transpiration rates and photosynthetic efficiency. CFD offers detailed insights into airflow and microclimate control, essential for managing these indicators effectively. CFD simulations help optimize the internal climate by modeling interactions between soil, crops, and the greenhouse structure, ensuring a balanced thermal and humidity environment crucial for crop health (Si *et al.*, 2023). Additionally, the management of solar radiation through greenhouse design significantly impacts crop exposure and photosynthesis, influencing growth and energy efficiency (Ray *et al.*, 2021),

(Mahjoob Karambasti *et al.*, 2022). The main objective of this study is to focus on the indoor climate distribution on a cultivated greenhouse condition with natural ventilation. It also investigates the effects of different solar radiation loads, with the novelty use of S2S radiation model coupled with local wind directions and profiles on the thermal comfort of the crops within the greenhouse. The study is numerically analyzed through the CFD model conducted by Star-CCM+ Software (Simcenter STAR-CCM+ Academic PowerOn Demand, 2021). Experimental measurements were used to verify the model's reliability. Given this main objective, a series of different scenarios was conducted to analyze the behaviour of crops in response to the thermal distribution due to different solar positions throughout the day in a naturally ventilated greenhouse.

2.2 Materials and Methods

2.2.1 Description of the case study

The study has been developed in the greenhouse of the Department of Agricultural and Food Sciences of the University of Bologna, Italy. The greenhouse is located in Imola (44.337340°N latitude, 11.718647°E longitude and 72m of altitude), the climate in Imola is classified as humid subtropical, with mild winters and hot summers. The town is situated in a basin and is surrounded by hills, which can have a significant impact on the local weather patterns. The greenhouse covers an area of 304.8 m^2 (12.7m wide, 24m long), see (Figure 2.1). The greenhouse consists of three spans (each one has a height of 4m at eave, and a maximum height of 5.5m, with 40% pitch slope) made of steel and covered by 4mm thick glass with a concrete ground, see (Figure 2.1).

The study was conducted in the middle span (12.7 m long, 8 m wide) which is separated from the two other spans by a glass wall and has a separated access door. The span is equipped with two continuous roof vents on both sides along the length of the span, with opening angle of 25°, these vents are crucial to guarantee the natural ventilation inside the greenhouse. The span has 4 Poly-carbonate benches, one bench was stocked with young sweet pepper (i.e. Capsicum annuum L.), potted in 10 cm high containers. The plants were uniformly placed in 150 pots and distributed in 6 columns on the bench (size of the bench 1.64m wide, 5.7m long, and 1.0m high). The plant density was 16.09 pots per m^2, average plant height was 15 cm. plants were watered on the second day of the experiment campaign. The layout of the greenhouse is showed in (Figure 2.1). The investigations have been focused on the middle span, highlighted in blue. The spans are completely independent from each others; therefore, the middle span ventilation is not affected by the opening of the surrounding spans.

2.2.2 Description of the numerical model

The utilization of Computational Fluid Dynamics (CFD) has significantly advanced the development of numerical models, facilitating the acknowledgement of the interactions between variables within the greenhouse microclimate. The CFD methodology solve the fundamental Navier-Stokes equations with the mass and energy conservation equations. (Kinyua, 2017). The CFD simulations are carried out by Simcenter STAR-CCM+ software(Simcenter STAR-CCM+ Academic PowerOn Demand, 2021). CFD tools allow simulating complex zones like agricultural structures with inner micro-climate and external environmental parameters. These zones can be defined as calculation domains, are

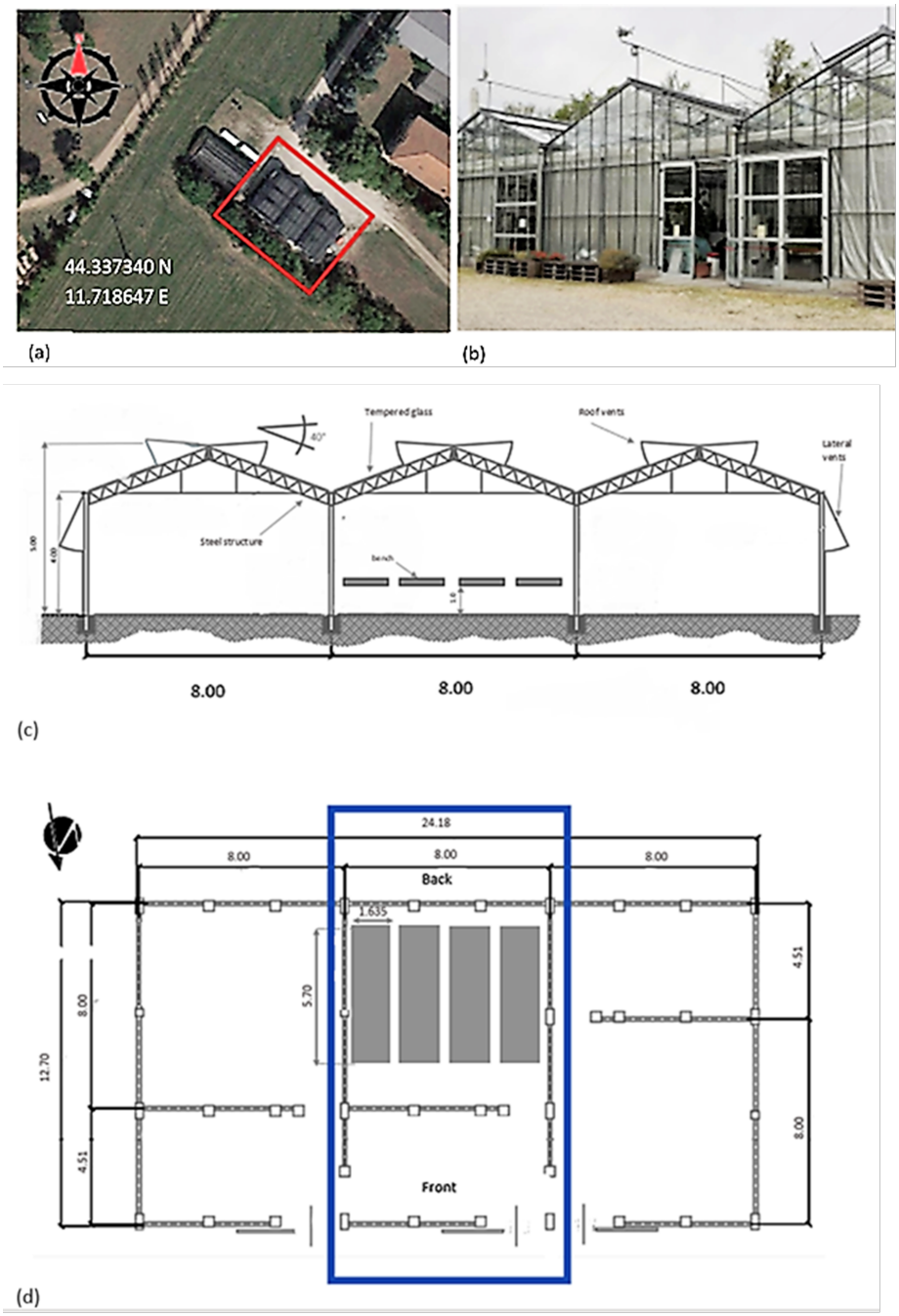

Figure 2.1: The case study greenhouse. (a) Map view, (b) lateral view, (c) vertical transverse section and (d) plan view of the layout with the blue rectangle indicating the bay considered in the study.

divided into elementary volumes, defined as cells to solve the conservation equations to predict variables such as pressure, velocity, and temperature. These variables are obtained in each control volume through an iterative procedure that continues until the nonlinear system of equations has a converged solution. The calculation domain has an area of 25661 m^2 with 27 m height, the domain includes the greenhouse, the floor, the benches, the pots and the plants. The geometrical domain was defined as an octagon to accurately symbolize the directions of airflow, the left side of the calculation domain represents the East, East-South and South side. A view of the domain adopted in the simulations is reported in (figure 2.2).

A polyhedral mesh was chosen to limit the numerical diffusion of errors and facilitate calculation convergence. In STAR-CCm+, a specific dualization scheme is used to automatically transform an underlying tetrahedral mesh into a polyhedral mesh. The polyhedral meshing model generates random polyhedral-shaped cells that are relatively faster and more efficient to build than a tetrahedral mesh for a given surface. The mesh was refined around the crops, benches and in areas where strong gradients may occur, i.e., near the ground and walls, see (figure 2.2).

2.2.2.1 Fundamental equations

The flow in the greenhouse is considered to be a steady state, incompressible and turbulent. The Navier-Stokes transport equation represents the distribution of the mass, velocity components, and temperature in the domain in Eq.(2.1):

$$\frac{\partial \phi}{\partial t} + \frac{\partial}{\partial x_j}(u_j \phi) = \frac{\partial}{\partial x_j}(\Gamma_\phi \frac{\partial \phi}{\partial x_j}) + S_\phi \tag{2.1}$$

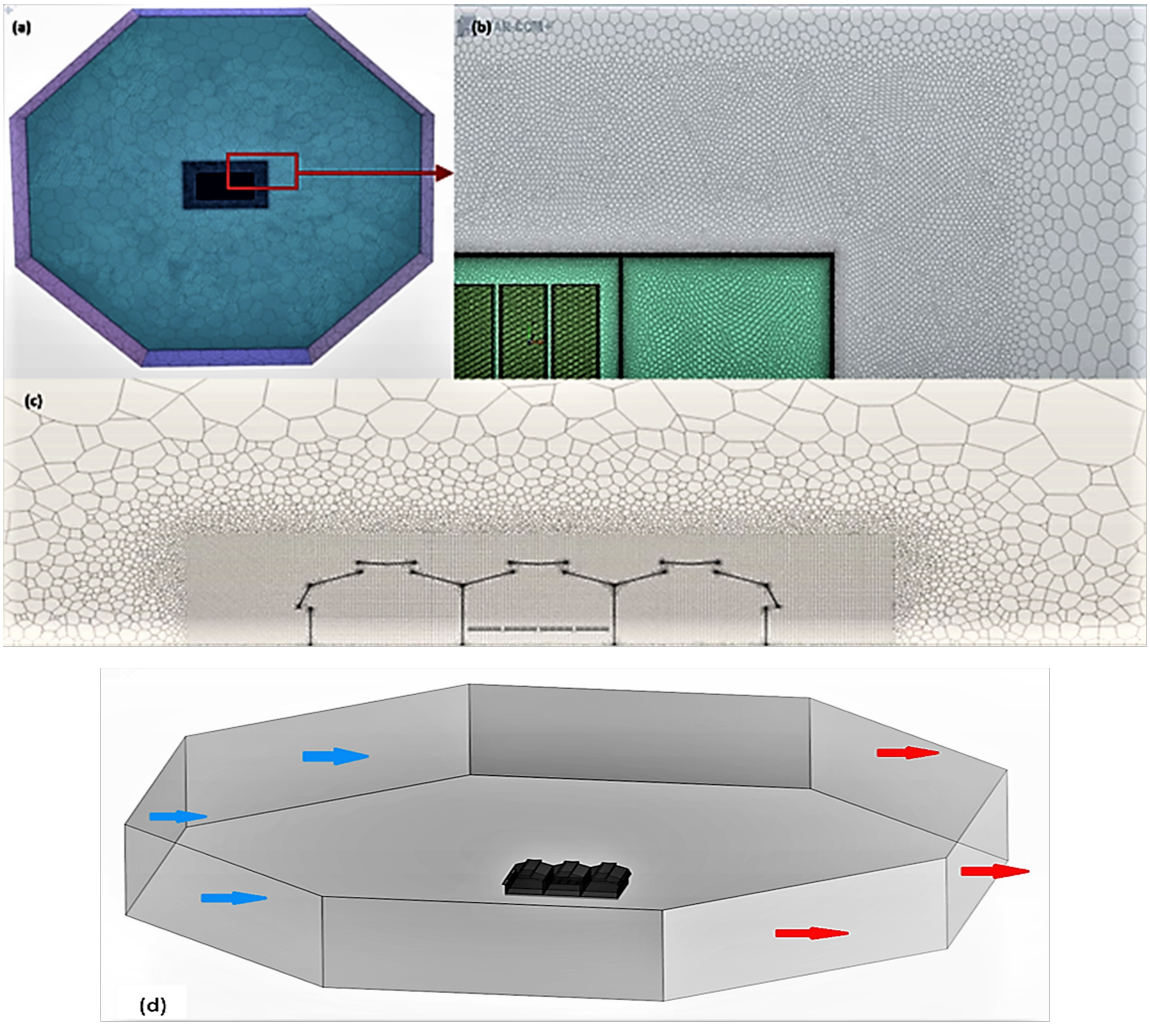

Figure 2.2: Numerical model used in the work. (a) Top view of the entire domain. (b) Detail of the mesh close to a corner of the greenhouse. (c) View of a vertical section of the mesh. (d) Geometrical computational domain including the greenhouse, inlets (South, South-East, East) indicated by the blue arrays and outlets (East, East-South and South) indicated by the red arrays.

where: u_j represents components of fluid velocity, Γ is the diffusion coefficient, and S_ϕ is the source term.

The standard *k*-ε turbulence model within the domain has been used ((Launder and Spalding, 1974)) which introduced the equations of kinetic energy *k* and the dissipation rate ε:

$$k = \frac{u_*^2}{\sqrt{C_\mu}}\left(1 - \frac{z}{\delta}\right) \tag{2.2}$$

$$\varepsilon = \frac{u_*^2}{kz}\left(1 - \frac{z}{\delta}\right) \tag{2.3}$$

respectively, where δ is the atmospheric boundary layer depth and C_μ is a coefficient used to define the eddy viscosity in *k*-ε models. A standard value of C_μ= 0.09 has been chosen. The equations were numerically solved according to the finite volume method using the CFD software STAR-CCM+. The convergence criteria for the continuity, momentum and energy was (10^{-6}) and was reached after 3000 iteration.

The boundary conditions derived from measurements were used to introduce the effect of outside parameters including air temperature, wind velocity, and air humidity, see Table (2.1). At the entrance of the calculation domain, see Figure (2.2), on the left side (South, South-East, East) a uniform temperature obtained from the weather station data was applied at the inlets, and the horizontal velocity profile was derived from the experimental data by using the log-law fit:

$$U(z) = \frac{u_*}{K} ln\left(\frac{z + z_0}{z_0}\right) \tag{2.4}$$

Where: U(z) is the horizontal velocity (m s^{-1}), u* is the friction wind velocity, K is the von Karman's constant, z is the height above the ground and z_0 is surface roughness. Uniform temperature and humidity obtained from the measurement were applied at the inlet. A no-slip wall boundary condition was applied to all walls in the domain including greenhouse walls, benches and ground. This condition assumes that the velocity of air particles at the boundary (wall) is zero, meaning that the fluid particles do not move relative to the wall. A convective boundary condition was applied on the soil inside the greenhouse with a heat transfer coefficient of 13 W$m^{-2}K^{-1}$. However, the soil outside the greenhouse was assumed to be adiabatic, as the focus of the study was on the microclimate inside the greenhouse. In order to ensure a parallel flow, a symmetry boundary condition has been imposed on the top side (sky) and the lateral sides of the calculation domain (North-East and South-West).

Radiation was simulated directly using the solar load feature built-in Star-CCM+, and was defined on all the regions, taking into account the geographical area of the greenhouse. In order to take account of the overhead heating, heat flux was applied on the greenhouse walls and along the ground surface. The CFD software automatically conducted the coupling between radiative and convective transfer for the solid and fluid interfaces, and the porous media was considered as a semi-transparent media interfacing with radiation. The software provided the radiative balance for each mesh of the porous media. The energy balance equation, which calculates the sensible and latent heat exchanges between each cell of the porous media and the air, used this global net radiative flux as its source term (Fatnassi *et al.*, 2017).

At the exit of the calculation domain (North, North-West, West), a pressure outlet con-

dition (atmospheric pressure) was imposed. Table 2.1 shows the values of the experiment measurements that used as initial boundaries and boundary conditions.

Table 2.1: Initial parameters and boundary conditions.

Parameters	Numerical Value
External air temperature C°	19.55
Inside air temperature C°	23.4
Concrete temperature C°	22.8
Cultivation bench temperature C°	28
Glass wall temperature C°	29.8
Inlet velocity profile m s^{-1} at (5) m	1.75
Convection heat transfer coefficient of greenhouse W$m^{-2}K^{-1}$	25
Greenhouse thermal resistance m^2K W^{-1}	0.2

2.2.2.2 Radiative Sub-Model

A radiative sub-model was activated in order to take account of the thermal contribution of radiative transfers between the surfaces in the greenhouse. The Surface to Surface (S2S) model was chosen due to its ability in simulating the radiation generated by the sun by using the Solar Calculator feature. The solar calculator is able to compute the direct and diffuse solar radiation depending on the geographical location of the greenhouse and the time of carrying out the experiments (Saberian and Sajadiye, 2019). The values of direct solar flux and diffuse solar flux obtained according to the greenhouse coordinates (44.337340°, 11.718647°) on the 29^{th} of April at 13:00, are 670 W m^{-2} and 220 W m^{-2}, respectively. The gray spectrum model considers the full length of the thermal spectrum as a simplified method to represent the environment around the continua, applying the gray model could effect the model accuracy but it has been selected as a compromise for the

computational time.

The thermal-radiative properties of the greenhouse's materials have been used in the model are shown in Table (2.2) and Table (2.3).

Table 2.2: Thermal characteristics of the materials used as initial conditions.

Material	Density (ρ) (kg m^{-3})	Thermal Conductivity (κ) (W $m^{-1}K^{-1}$)	Specific heat (C_p) (J $kg^{-1}K^{-1}$)
Glass	2530	1.2	840
Poly-carbonate	1200	0.2	1170
Soil	1620	1.3	1480
Concrete	2200	1.5	1000

Table 2.3: Radiative characteristics of the materials used as initial conditions.

Material	Absorbance	Emissivity
Glass	0.7	0.9
Poly-carbonate	0.1	0.9
Soil	0.9	0.925
Concrete	0.6	0.88

2.2.2.3 Crop Model

The effect of the crops within the greenhouse has been modelled as momentum sink (related to the drag force on the leaves). The crops have been modelled as a homogeneous porous medium which creates a pressure drop based on Darcy-Forchheimer law (Boulard and Wang, 2002). This pressure drop is considered as a negative source term in the momentum equations. The sink of momentum due to the drag effect by a crop unit volume can be evaluated by means of the well-known equation (Thom, 1971).

$$\mathrm{S} = -\,\rho_{\mathrm{a}}\,\mathrm{LAD}\,\mathrm{C_D}\mathrm{V}^2 \tag{2.5}$$

where LAD is the leaf area density ($m^2\ m^{-3}$),V is the air velocity, ρ_a is the air density (kg m^{-3}), and C_D is the dimensionless drag coefficient. With reference to (**?**), a sweet pepper crop cultivated in a greenhouse, has value of drag coefficient equal to C_D = 0.31, and LAD = 6 ($m^2\ m^{-3}$) as Molina-Aiz had empirically measured in an experimental wind tunnel for four crops including sweet pepper crops.

2.2.2.4 Energy balance model

The porous medium representing the crops was divided into elementary volumes to model the heat transfers between the crops and the greenhouse indoor environment. Since that sweet pepper crops are cultivated in pots on benches, conductive transfers between the benches and the crops can be neglected (Kichah *et al.*, 2012). The energy balance depends on environmental factors, most importantly solar radiation, humidity, air temperature, and air velocity. In this study, as the code StarCCM+ does not have an integrated model to simulate the energy balance, a user-defined function (UDF) was built to compute heat and resistances, for each cell in the crop boundary zone. A radiative flux reaches each elementary volume and converts it into latent heat flux and sensible heat flux.

$$G_a = Q_s + Q_l \tag{2.6}$$

where G_a (W m^{-3}) is the radiative flux absorbed by each cell in the porous media, Q_s (W m^{-3}) is the sensible heat flux at the canopy level and represents the heat flux transferred between the crops (porous media) and the air in the greenhouse, and Q_l (W m^{-3}) is the latent heat flux that represents the transpiration process. The sensible heat flux produced

by the crops can be expressed as (Fatnassi *et al.*, 2017):

$$Q_s = LAD\ \rho_a\ C_p\ (T_l - T_a)\ /r_a \tag{2.7}$$

where r_a is the leaf aerodynamic resistance considered to be r_a=271 (s m^{-1}) following (Baille *et al.*, 1994), ρ_a is the air density (kg m^{-3}), C_p is the air specific heat at constant pressure (J $kg^{-1}\ k^{-1}$), T_a is air temperature,and T_l is the leaf temperature. Following (Bouhoun Ali *et al.*, 2018) the latent heat flux can be expressed as:

$$Q_l = \lambda LAD\rho_a\ \frac{(w_L - w_a)}{(r_a + R_s)} \tag{2.8}$$

where λ is the latent heat of vaporization of water set as 2500 (kJ kg^{-1}) following (Bouhoun Ali *et al.*, 2014), w_L and w_a are the absolute humidity of leaf and air (kg kg^{-1}), and R_s is the leaves stomatal resistance (s m^{-1}), it plays a crucial role in the transpiration flux, and can be defined as a function of global radiation and vapor pressure deficit, following (Zhang and Kacira, 2022) it can be expressed as:

$$R_s = 200\ \frac{(31 + G_a)[1 + 0.016(T_a - 16.49)^2]}{6.7 + G_a} \tag{2.9}$$

2.2.3 Experimental set-up

Measurements were undertaken for three days (28th, 29th, 30th) of April 2021. Inside the greenhouse, a set of sensors were placed for providing inputs and data, to validate the CFD model, and to check the interaction between the crop growth and the indoor conditions. Two hot wire anemometers Delta Ohm, with uncertainty of $0.01 \mathrm{m} s^{-1}$ were used to

monitor the wind velocity and temperature located on different heights and positions. The measurements points M1, M3 and M5 were taken at 10cm above crop level, and M2, M4 and M6 were taken at 20 cm above the crop level, as shown in Figure 2.3a. The anemometers also used to measure the velocity and temperature around the side of the bench at 90 cm and 1.10 cm above the ground represented in M7, M8, M9, M10 in the positions shown in Figure 2.3a.

The temperature, T_a, and the relative humidity (RH) of the air were measured by using 5 probes (i.e. dataloggers) located on the surface of the benches, and above the benches. The leaf temperature, T_l, and the ground temperature were recorded by using a thermal camera (AVIO) as well as the temperature of the walls, see Figure 2.3b. All the above mentioned parameters were measured every 5s and averaged over a 10 min period. The measurements for this study were taken during the day between (10:00 am and 4:00 pm). The outdoor wind speed, wind direction, air temperature, solar radiation and air humidity measurements were taken from the weather station located on the top of the greenhouse.

2.3 Results and discussion

A first set of simulations has been done to verify the model by a comparison with the data obtained by the experimental measurements. Then, the optimal conditions for the thermal comfort of the plants were defined for six different meteorological configurations.

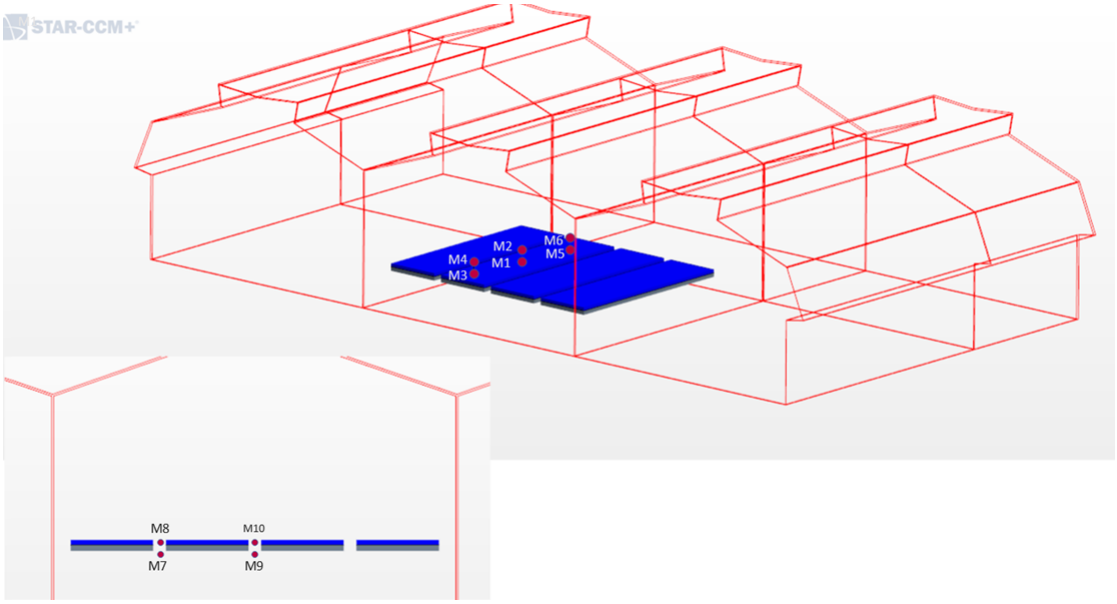

(a)

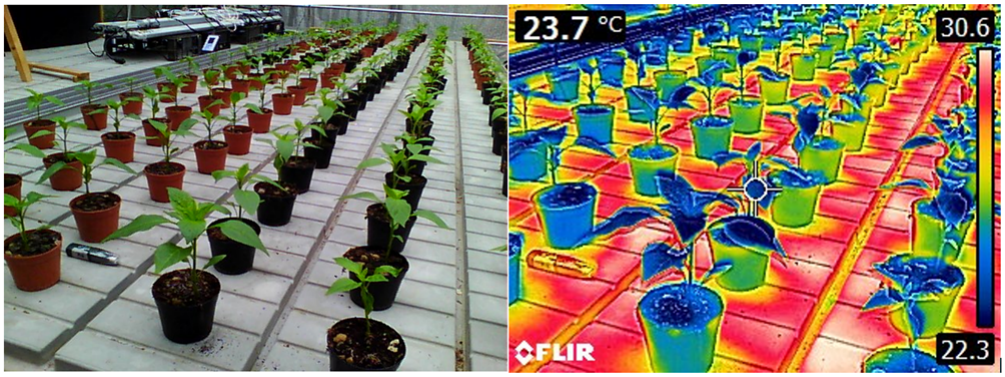

(b)

Figure 2.3: Experimental measurements: (a) measurement points highlighted by red points; (b) temperature measurements with thermal camera.

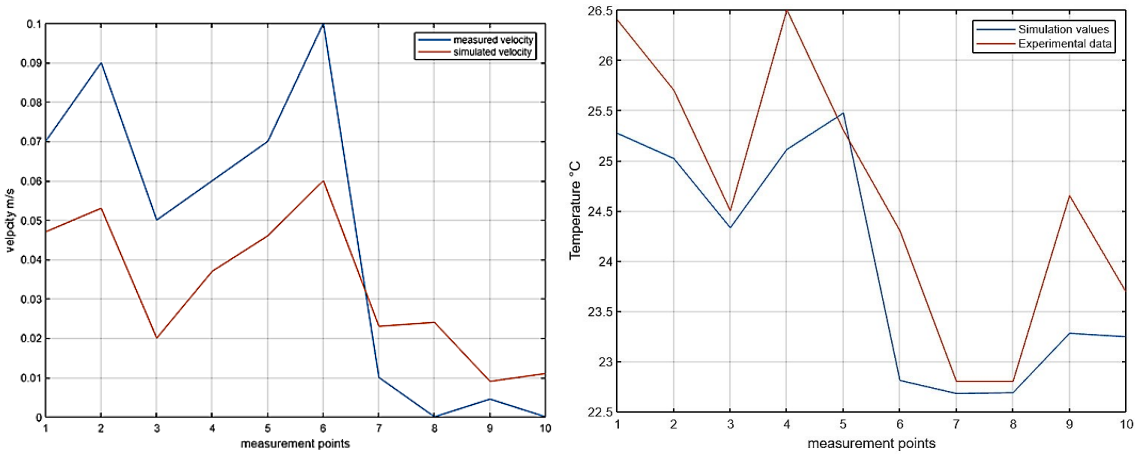

(a) Velocity (b) Temperature

Figure 2.4: Comparison between measured and simulated (a) air velocity and (b) air temperature.

2.3.1 Numerical model validation

The experimental data used for the validation have been taken from the second day of the campaign, the 29th of April, 2021 at 13:00 as the weather was more stable with partial clouds.

It is observed from Figure 2.4a and Figure 2.4b that the results of the simulation had good agreement with the experimental ones, the highest difference in temperature was 1.5°C at point M6. Similarly, the velocity maximum difference was 0.04 m s^{-1} also at point M6, considering the highest difference of temperature and velocity occurred at the same point of measurement, it may have been caused by an experimental error.

The distribution of the temperature on the crops was heterogeneous with a difference in temperature up to 3 ^{o}C, due to the combined influence of radiation and convective heat transfer, as shown in (figure 2.5a). The vertical distribution of crop temperature is hardly noticeable due to the low height of the porous media.

The simulated air velocities of the 10 points of measurement have also been compared

with the corresponding points in the experiment. The wind velocity has a non uniform distribution inside the greenhouse, combined with a vortex in the middle of the span, with other two small vortices on the sides of the span, see Figure 2.5b. The airflow above the crops has a velocity range around 0.2 m s^{-1}, while the airflow passing through the porous media has a lower velocity due to the impact of crops.

The reliability of the numerical model was evaluated using the Root Mean Square Error (RMSE), which demonstrated a favorable agreement between the simulated and measured data, the RMSE of the temperature and air velocity were 1.01 °C and 0.05 m s^{-1}. These RMSE values shows alignment with the results reported in previous studies, (Bouhoun Ali *et al.*, 2018) obtained RMSE values of 0.49 °C for temperature and 0.05 m s^{-1} for air velocity, and (Teitel *et al.*, 2022) reported RMSE range of [0.86 - 1.57]°C for the temperature through different cases. The comparison of overall results demonstrates a good agreement between the simulation and the experimental test. The CFD model is capable of performing realistic simulations of the micro-climate inside the greenhouse related to the thermal contribution of solar radiation. The porous media model can reliably simulate heat and mass transfer between the plants and the surrounding environment.

2.3.2 Model applications

Once the model was validated, it could reliably be used to predict solar radiation distribution with different sun positions at different seasons. Since the values of direct and diffuse solar irradiation change with the sun altitude (PVGIS, 2020), analysis of different solar positions throughout the day has been carried out on four cultivated benches in the middle span of the greenhouse. Six different scenarios have been selected to represent these

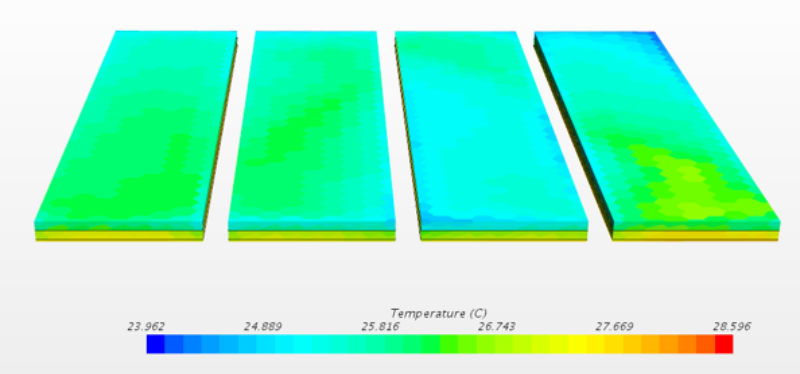

(a)

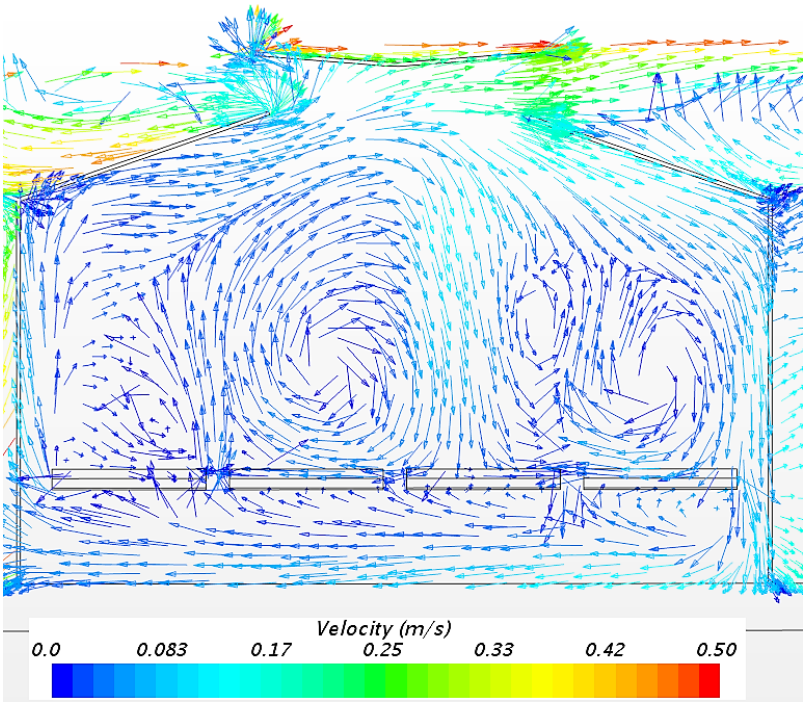

(b)

Figure 2.5: View of (a) temperature distribution of the porous media. (b) Vertical section at the middle of the benches showing the vector distribution of the velocity.

variation along with changing in the temperature and the wind speed.

Table 2.4: Summary of the six cases considered in the study.

case number	simulated time	sun position to greenhouse	outside temp. °C	inlet velocity profile ms^{-1}	direct solar flux Wm^{-2}	diffuse solar flux Wm^{-2}
1	12:00	vertical	33	1.75	947	237
2	19:00	diagonal	29	1.75	103	26
3	00:00	no sun	26	1.75	zero	zero
4	12:00	vertical	33	4	947	237
5	19:00	diagonal	29	4	103	26
6	00:00	no sun	26	4	zero	zero

The six configurations have been divided into two groups. The first group has a velocity profile of 1.75 m s^{-1} at the inlet with three different settings of sun position, at noon where the sun is vertical to the greenhouse with 63° elevation with reference to the horizon, when the sun is diagonal to the greenhouse with 15° elevation, and at midnight when there is no impact of the sun.

The second group has a velocity profile of 4 m s^{-1} at the inlet, to investigate the effect of wind velocity on the temperature distribution inside the greenhouse, with the same configurations of sun positions applied to the first group.

2.3.2.1 Analysis of air temperature distribution

In general, the temperature pattern in the six cases reveals that the greenhouse microclimate is warmer than the external environment and the roofs vents work as inlet for the cold air coming from outside the greenhouse and as outlet for inside warm air. The temperature distribution in the vertical cross-section in the middle span of the greenhouse shown by Figure 2.6 demonstrates the higher heat transfer values on the glass walls, soil, and ground, which are related to higher surface heat transfer coefficient on these regions.

The observed temperature in the first group (i.e. cases 1, 2, and 3) with a wind velocity profile of 1.75 ms^{-1} is higher if compared to the second group (i.e. cases 4, 5, and 6) with 4 ms^{-1}, as shown by Figure 2.6.

The significant difference in temperature is noticed in case 1 and case 4, the highest increase is in case 1 of about 5°C with reference to the external conditions, due to the high thermal load and the low wind velocity, see Figure 2.8.

In cases 2 and 5, the temperature has a moderate distribution due to less thermal load on the greenhouse. The temperature between the crops and the surrounding air is in the same range. It is noticeable that the soil on the benches in case 2 is warmer than case 5 due to lower wind velocity.

In cases 3 and 6, when the effect of solar radiation is absent, the overall temperature of the greenhouse is decreasing mainly because of radiative losses. The temperature inside the crops is warmer than the air around it. In case 3, the difference in temperature between the crops and the surrounding air is 2 °C, while in case 6, the difference is slightly around 1 °C, due to the higher wind velocity.

2.3.2.2 Airflow patterns

Velocity was calculated for each case through a vertical line in the middle of the span. The measurement line starts from the ground, passes through the porous media zone and reaches the roof. Analysis of the results according to their height and comparing the data with the flow patterns, indicates that the roof vents work as inlet and outlet to the span. The wind flow is facing the drag force of the porous media, in addition to the presence of benches which strongly decrease the wind velocity. (Figure 2.7) illustrates the average

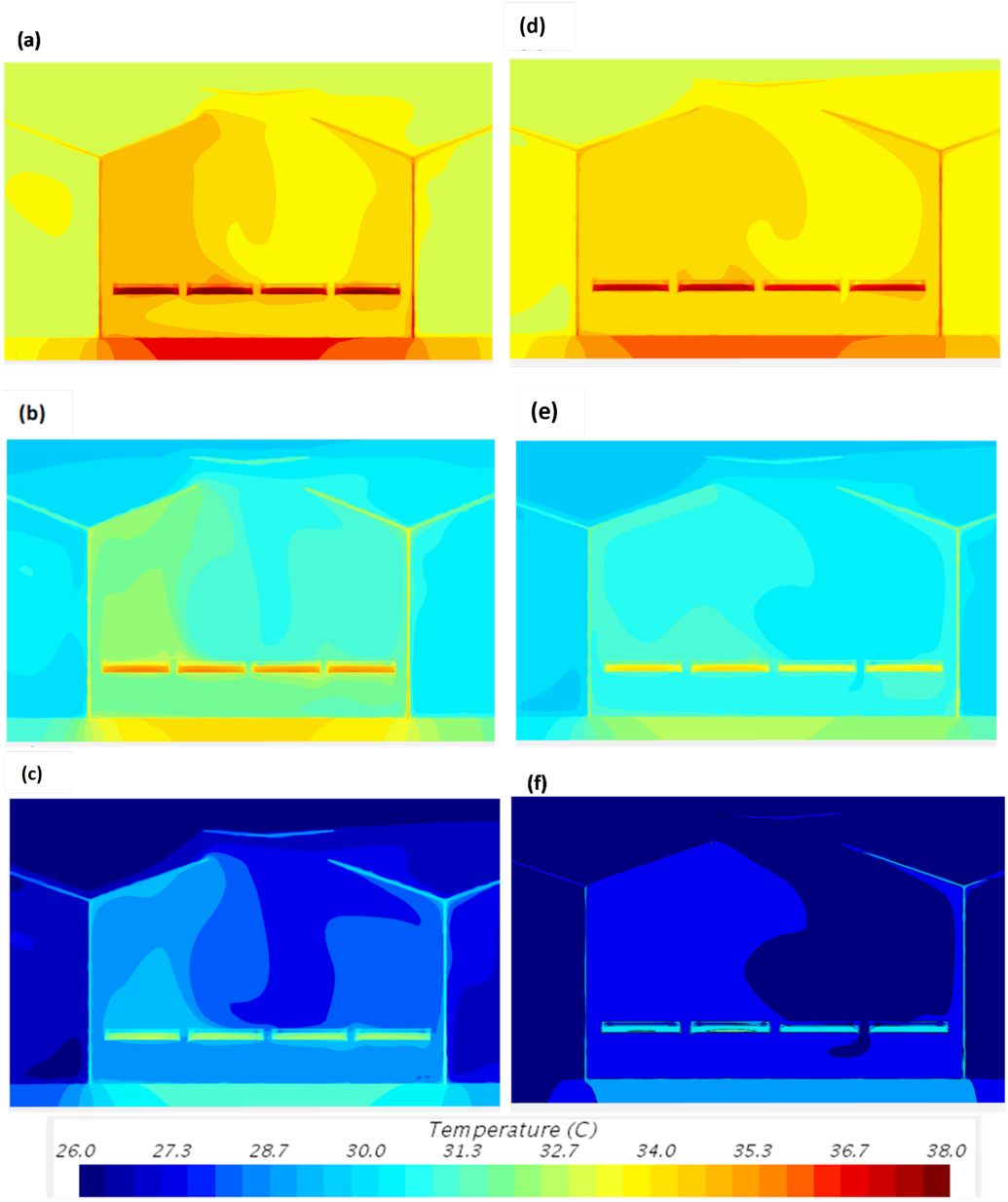

Figure 2.6: View of the vertical temperature distribution at the middle span: (a) case 1, (b) case 2, (c) case 3, (d) case 4, (e) case 5, (f) case 6.

wind velocity according to the height inside the middle span.

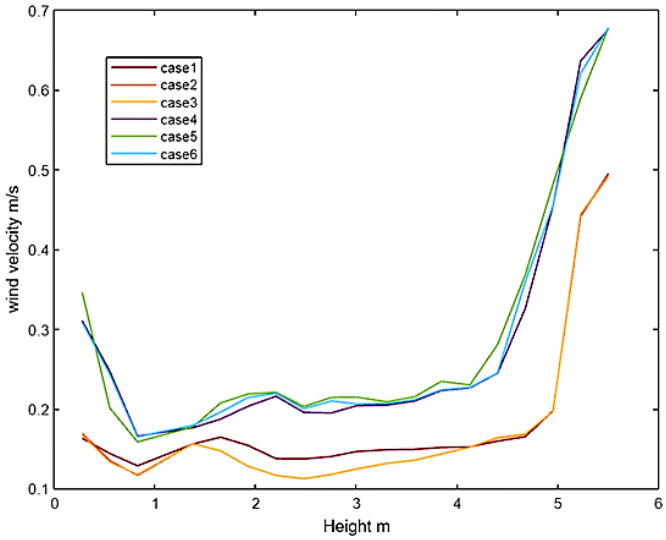

Figure 2.7: Average wind velocity for the six cases in the middle span, at 9 m from the north side (front) and 11 m from the east side of the greenhouse.

Case 6 has the highest wind velocity near the roof vents and it takes a similar pattern as Case 4 and Case 5, the velocity decrease directly with height of the greenhouse except in two places, at 2.5 m where the air current is being fed by the vortex (as have been seen previously in (figure 2.5b)), and near the ground as the air current is being fed by direct airflow coming from the windward wall and goes beneath the benches. Case 2 and Case 3 have no numerically considerable difference according to their average wind velocity. For Case 1, Case 2 and Case 3, which have a wind profile of 1.75 m s^{-1}, the results indicate that the wind distribution around the crops could hardly reach the crops minimum range for the optimum growth [0.2 - 0.7] m s^{-1}. For cases 4, 5 and 6, with a wind profile of 4 m s^{-1}. The overall results closely align with previous findings, (Zhang and Kacira, 2022) reported a velocity range of [0.2 - 0.5] m s^{-1}, and (Roy and Boulard, 2005) obtained a velocity range of [0.2 - 1.5] m s^{-1}. The results indicate that the wind distribution fits the

requirements for the crops optimum growth.

2.3.2.3 Characterization of crops thermal comfort

The investigation of the thermal comfort of plants within a greenhouse requires the establishment of a baseline for the optimal range of temperature and airflow that correspond with crop physiological tolerance. Studies such as (Upadhyay *et al.*, 2023) have emphasized the importance of defining regional baselines for thermal comfort that consider microclimate conditions and crop types.

The simulation results revealed that under conditions of high solar radiation specifically when temperatures reached 33°C and the direct solar radiation flux was 947 Wm^{-2} (cases 1 and 4) the airflow passing through roof vents significantly reduced the temperature at the crop level by approximately 2°C (see Figure 2.8). This demonstrates the critical role of ventilation in managing heat stress in greenhouses. Particularly in case (4), where higher air velocities were recorded, there was a maximum temperature reduction of about 4°C at the crop level, indicating that air velocity has an important role in enhancing temperature uniform distribution among the crops.

However, during periods of low solar radiation (i.e. cases 2 and 5) where the temperature was 29°C and the solar radiation flux was 103 Wm^{-2}, or in scenarios with no solar radiation at all (i.e. cases 4 and 6) with temperatures at 26°C, the effect of air velocity on thermal comfort was less noticeable. This indicates that in cooler conditions, less air movement is required to maintain comfort levels, aligning with the findings from the literature that emphasize the importance of adjusting environmental controls to suit specific physiological needs of crops (Piscia *et al.*, 2015).

Furthermore, maintaining optimal temperature and humidity is essential to prevent plant stress and disease, which is consistent with the literature acknowledging the importance of these factors in greenhouse management (Torres and Lopez, 2011), (Elkins and Van Iersel, 2020). This study's findings on the importance of airflow in temperature regulation support the concept that dynamic adjustments to air circulation are critical in preventing pathogen buildup and ensuring plant health (Nonomura *et al.*, 2014).

The analysis of various cases within this study provides a foundational understanding that can be utilized to develop a digital twin of the greenhouse. This digital model could serve to refine greenhouse designs and enhance dynamic control of the environmental conditions, thereby optimizing the thermal comfort of crops in existing facilities.

2.4 Conclusions

A CFD model, with novel modeling elements such as the S2S radiation model coupled with thermal and plant models integrated in this software, was used to numerically investigate the effects of different solar radiation loads, local wind directions and profiles, and indoor climate on a cultivated greenhouse with natural ventilation. An experimental measurement set-up was used to verify the model's reliability. The CFD model was proven to be an effective method for simulating the crops as a porous media that is able to represent heat transfer between the plants and the surrounding environment, and forecasting solar heat load and temperature distribution inside the greenhouse. The results seem to indicate that by increasing wind velocity, the temperature distribution becomes more homogeneous inside the span, the porous media temperature decreases by approximately 3°C compared

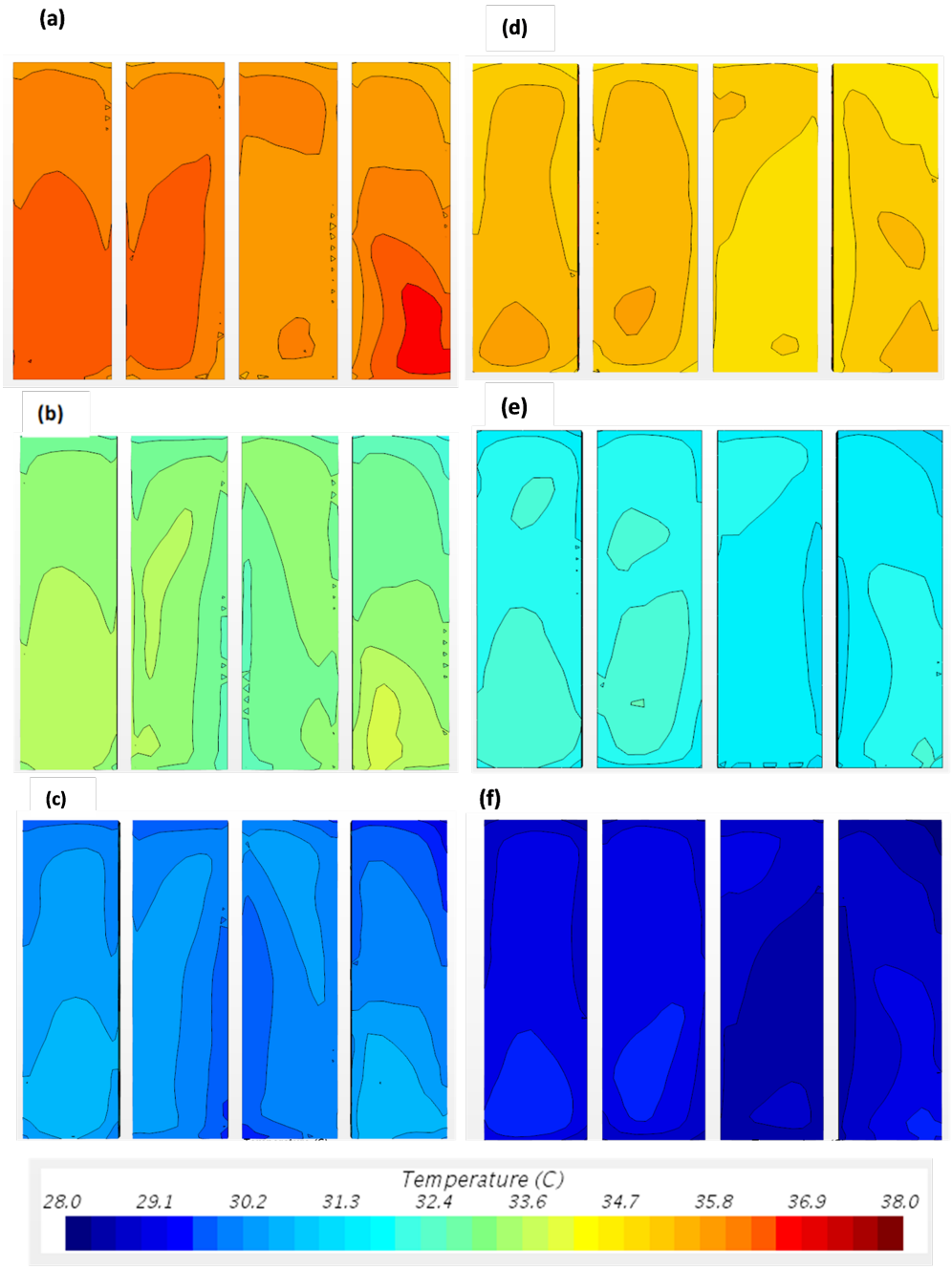

Figure 2.8: Top view of benches showing temperature distribution at the crop level: (a) case 1, (b) case 2, (c) case 3, (d) case 4, (e) case 5, (f) case 6.

to the cases with lower velocity. The CFD also investigated the influence of the crops on the indoor climate, as the porous media works as obstacles to the wind flow leading to form several vortices with lower velocities. The results exemplify the appropriate micro climate conditions to reach the thermal comfort of the crops in an energy-efficient greenhouse by depending on the natural ventilation and solar radiation. Analysis of the crops temperature and the air velocity around the crops through different test cases to find the thermal comfort range is achieved to meet the crops best thermal conditions.

Chapter 3

Assessment of the influence of canopy morphology on leaf area density and drag coefficient by means of wind tunnel tests

3.1 Introduction

The aerodynamic parameters of the crops characterize the effect of the canopy on air flow, these parameters include the drag coefficient and the leaf area density (LAD) (Burger, 1992). In order to evaluate the impact of crops on the air flow and exchange processes of momentum and climate parameters including heat, water vapor, and CO_2, it is crucial to understand the drag force produced by plants.

Several researches indicate that drag coefficient depends on the type of plant, canopy density, porosity, and shape of leaves and their flexibility. This diversity suggests that a one-size-fits-all approach is insufficient for accurately capturing the complex interactions between plant canopies and air flow. Therefore, the experimental tests available in literature aiming to determine the drag coefficient have been accomplished through a direct method to calculate the drag force on crops (Dexin *et al.*, 2003) or, in those cases in which is possible to neglect the impact of crops on turbulent flow, by measuring the velocity and the pressure drop (Molina-Aiz *et al.*, 2006).

In greenhouse CFD modeling (Santolini *et al.*, 2022), (Al-Rikabi *et al.*, 2023), the crop canopy is modeled as a simplified equivalent porous medium and the canopy effects on the airflow are modeled as an average for the volume of the canopy. The pressure and viscous forces generated by canopy elements, i.e. leafs and branches, result in a rise of the momentum sink causing a reduction in the air flow (Sase *et al.*, 2012). The drag coefficient, which is necessary to model the crop canopy as an equivalent porous medium, is often considered as a constant of the aerodynamic properties of the crops, irrespective of wind speed, or crop species (Buccolieri *et al.*, 2018). However, recent studies have begun to challenge this assumption, emphasizing the need for more detailed information of how different crop species and varying wind conditions affect the drag coefficient.

On the other hand, it has been observed that the CFD model reliability is strongly related to the adopted drag coefficient value (Pinard and Wilson, 2001) and the accuracy in the estimation of fluid flow and of downstream air velocity values depend on the assumed drag coefficient. Several studies have investigated the crop influence on air flow inside the greenhouse through wind tunnel measurements. Wind tunnel test is an effective method

to investigate the aerodynamics of air flow through vegetation (Zhang and Kacira, 2022), (Endalew *et al.*, 2009). In fact, wind tunnels create a controlled environment that makes it possible to conduct in-depth research on how crop characteristics like porosity and flexibility affect the drag coefficient value (Gillies *et al.*, 2002). These studies are crucial in filling the gap between theoretical models and practical, real-world applications.

(Manickathan *et al.*, 2018) research extended the application of wind tunnel experiments beyond small crops, focusing on trees in urban environments, and investigated how well small-scale tree models can replicate the aerodynamic behavior of larger, real-life trees by comparing their drag coefficients and turbulent flow patterns. Implementing larger vegetation types like trees highlights the wide-ranging applicability and potential of wind tunnel experiments in various environmental research areas.

These highly controlled tests provide us a firm understanding of how crop canopy affects the drag coefficient. Therefore, the wind tunnel tests can provide the necessary information to strengthen the reliability of equivalent CFD models, the latter allowing for a more precise evaluation of the effects of vegetation on the microclimate (Molina-Aiz *et al.*, 2006), (Burger, 1992), (Endalew *et al.*, 2009), (Dexin *et al.*, 2003). By enhancing our knowledge of these interactions, such models can become powerful tools in environmental management and urban planning.

Different studies indicated that the drag coefficient change with crop species, amount of vegetation, and the porosity of plants(Koch *et al.*, 2018), (Beckett *et al.*, 2000). Another considered aspect is the impact of changes in the canopy morphology on the airflow field of the spray (Lazzaro *et al.*, 2008).

Thereby, in the present paper, the drag coefficient has been experimentally obtained through

tests on two crop species with different morphological features, since the porosity plays the major role in the aerodynamic effects of the crops. The crop species under study are two small aromatic plants, Basil (i.e. *Ocimum basilicum*) and Mentuccia (*Clinopodium nepeta (L.) Kuntze*). This choice of species allows for an investigation into how different plant structures, particularly in terms of leaf configuration and canopy density, impact aerodynamic parameters. The research aims at providing more insight in the accurate aerodynamic characterisation of vegetation useful for the calibration of equivalent volume of models to be used for solving complex CFD simulations. This is especially relevant in scenarios where precision is crucial, such as in the analysis of wind flow in urban green spaces or in smart farming. The approach adopted in this paper is significantly general, and the results can be highly effective in defining a pipeline for CFD simulations related to crop modeling. It's particularly applicable in scenarios such as plant production in greenhouse buildings, analyzing the behavior of green infrastructures, and designing nature-based solutions. These applications demonstrate the broad potential impact of this research in both agricultural and urban environmental contexts.

3.2 Materials and Methods

3.2.1 Theoretical consideration

The crops could be considered as a porous media, characterized by a solid matrix with interconnected pores. The flow within the porous medium is described by the Darcy law, which relates the pressure gradient ∇p to the volume-averaged velocity vector (u) in the

control volume.

$$\nabla p \;=\; -\phi\,\frac{\mu}{K}u \tag{3.1}$$

Where: K is the permeability of the porous medium which is independent of the nature of the fluid and depends on the pore geometry in the medium, ϕ is the porosity of the medium and μ is the viscosity of the air. This relationship forms the basis of modeling the movement of air through crop canopies, allowing for the prediction of airflow behavior in agricultural environments. While Darcy law represents Newton's second law of motion, its limitation lies in the absence of the inertial term u^2. This limitation becomes particularly noticeable at higher fluid velocities, where inertial effects cannot be ignored. To address this issue, Darcy-Forchheimer equation is used, incorporating a quadratic term.

$$\nabla p = \left(\frac{\mu}{K}u + \frac{C_f\,\rho}{K^{1/2}}u^2\right) \tag{3.2}$$

The equation introduces a dimensionless inertial factor C_f, which represents the non-linear momentum loss coefficient, and the fluid density ρ (kg m^{-3}). This enhancement allows for a more comprehensive modeling of airflow, especially in scenarios involving turbulent conditions. Notably, the value of C_f depends on the airflow direction with respect to the leaves. To determine the validity domains of the Darcy and Darcy-Forchheimer laws, a modified Reynolds number Re_m is employed.

$$\mathrm{Re}_m = \;\frac{u\;K^{1/2}}{v} \tag{3.3}$$

Where: *v* is the kinematic viscosity of the fluid ($m^2\ s^{-1}$), u is the fluid velocity (m s^{-1}), and $K^{1/2}$ corresponds to the characteristic dimension of the porous medium (i.e., dimen-

sion of the average pore). The application of this Reynolds number helps in identifying the appropriate model to use based on the specific conditions of airflow through the crop canopy. The Darcy law is valid when $Re_m < 1$. However, if $Re_m > 1$, the linear term is not constant and can vary based on the medium's porosity and the characteristic air speed. This variation is crucial for accurately predicting air flow in more turbulent conditions typically found in outdoor agricultural environments. For high Reynolds numbers $Re_m > 10$, the momentum sink can be expressed as a source term in Navier-Stokes Equation (Thom, 1971).

$$\nabla p = -\rho \, LAD \, C_D \, u^2 \tag{3.4}$$

Where: LAD is the leaf area density ($m^2 \; m^{-3}$) and represents the ratio of the total leaf area to the total volume of the crop cover, C_D is the drag coefficient and can be defined as the ratio of the pressure difference of windward and leeward and the dynamic force (Bitog *et al.*, 2011), and u is the air velocity. Integrating LAD into the Navier-Stokes equation allows for a more precise estimation of the impact of leaf density on airflow dynamics. By combining the equations related to the Darcy-Forchheimer Eq.(3.2) and the drag effect Eq.(3.4) it provides:

$$\frac{C_f}{K^{1/2}} = LAD \, C_D \tag{3.5}$$

Then, the calculation of the drag coefficient C_D can be achieved through the measurement of pressure loss across a vegetation canopy for various air velocities. This methodology is key for accurately quantifying the aerodynamic resistance offered by different crop types,

which is essential for precise simulations and predictions in CFD models. These models can then be applied to a variety of practical scenarios, ranging from optimizing crop arrangements for airflow in greenhouses to improving the design of urban green spaces for enhanced microclimate control.

3.2.2 Wind tunnel test

An open circuit wind tunnel built in the Department of Industrial Engineering of the University of Bologna has been used for carrying out the experimental tests. The utilization of a wind tunnel enables the possibility to have a regulated environment in terms of temperature and airflow velocity. This control is crucial to ensure that the tests reflect a consistent and repeatable set of environmental conditions, eliminating external variables that could affect the results. As shown in Figure 3.1, the wind tunnel test chamber has a dimensions as $30 \times 30 \times 60$ cm. The wind tunnel parts start by a contraction section of a 90 cm honeycomb as an inlet, attached to a channel that leads directly to the test chamber. This design facilitates a smooth and uniform airflow into the test section, which is essential for accurate aerodynamic measurements. A narrow channel follow the measurements chamber connected to the fan, the outlet of the wind tunnel. The airflow in this system is provided by the fan having a diameter of 45 cm with output rotation frequency ranging from 0 Hz to 50 Hz. The measurements in the wind tunnel were performed in order to calculate the drag coefficient C_D of the crops.

A calibration curve of the system has been conducted before starting the measurements on crops, in order to understand the relation between the fluid (i.e. air) velocity and the fan rotation frequency, and also to ensure the accuracy of the velocity measurements and

Figure 3.1: wind tunnel used for calculating drag coefficient for crops.

to establish a reliable baseline for interpreting the experimental data.

The measurements have been started after reaching a constant airflow. 24 readings of static pressure and dynamic pressure have been collected using a Pitot tube probe and a micromanometer (DP-Calc Micromanometer, Model 8715) with an accuracy of ± 0.01 ms^{-1}. The measurement interval was 5s. This high level of precision in pressure measurements is essential for calculating the drag coefficient with the necessary accuracy. The measurements have been carried out under different frequencies of the fan, beginning from 5 Hz and increased 5 Hz every reading until it reached 30 Hz. This range of frequencies

was chosen to simulate a variety of wind conditions that crops might encounter in horticultural settings. For each test point, the mean value of the 24 collected data has been calculated and then considered. Thirty readings of air velocity measurements at 2s interval were obtained by the same instrument and have been measured by placing the Pitot tube in upstream 190 mm away from the test chamber and also 190 mm in the downstream. This positioning ensures a comprehensive assessment of the airflow both before it encounters the crop canopy and after it has passed through, offering insights into the aerodynamic effects of the crops.

The experimental investigation involved three phases aimed at studying the density variation and analyzing the irregular shape and porosity of the canopy. Each phase involved different configurations of crops within the test section. In the first phase, a single Basil pot was placed in the test section, and measurements were performed at the leaves level (see Figure 4.1). This initial phase provides baseline data on how a single plant affects airflow, which is fundamental for understanding the cumulative effects observed in later phases. To assess the impact of different frontal areas, the Basil pot was rotated by 90° and the measurements were repeated. The second phase consisted of two Basil pots placed in the test section, while the third phase involved three pots within the test chamber. Similar to the first phase, measurements were taken at the same point, and crop rotation was implemented to treat the combined crops as a canopy. The subsequent phases allowed for the observation of how increasing canopy density influences aerodynamic properties.

To ensure optimal conditions for the crops, they were proper watered until the day prior to the tests. The measurement setup was conducted rapidly to minimize the possibility of wilting leaves and maintain the health of the crops throughout the experiments. This

(a) Basil (b) Mentuccia

Figure 3.2: Measurement positions indicated by blue arrays

consideration is critical, as the physical state of the plants could significantly impact the aerodynamic properties being measured. The entire experimental setup was then replicated for the Mentuccia crop to enable a comparative analysis. This replication with a different species provides a broader understanding of how various types of vegetation interact with airflow, enhancing the applicability of the study's findings.

3.2.3 Images elaboration

The porosity value has been determined by analyzing the image through the use of ImageJ software (Martin *et al.*, 2021), which has proven effective in measuring leaf area (Borges *et al.*, 2023). ImageJ is known for its versatility and precision in image analysis and offers a range of tools that are ideal for quantifying complex plant structures. Prior to conducting the wind tunnel tests, images were captured to distinguish the frontal area of the crops in a still air environment. This step is crucial as it ensures that the plant's natural posture and

structure are accurately represented in the analysis.

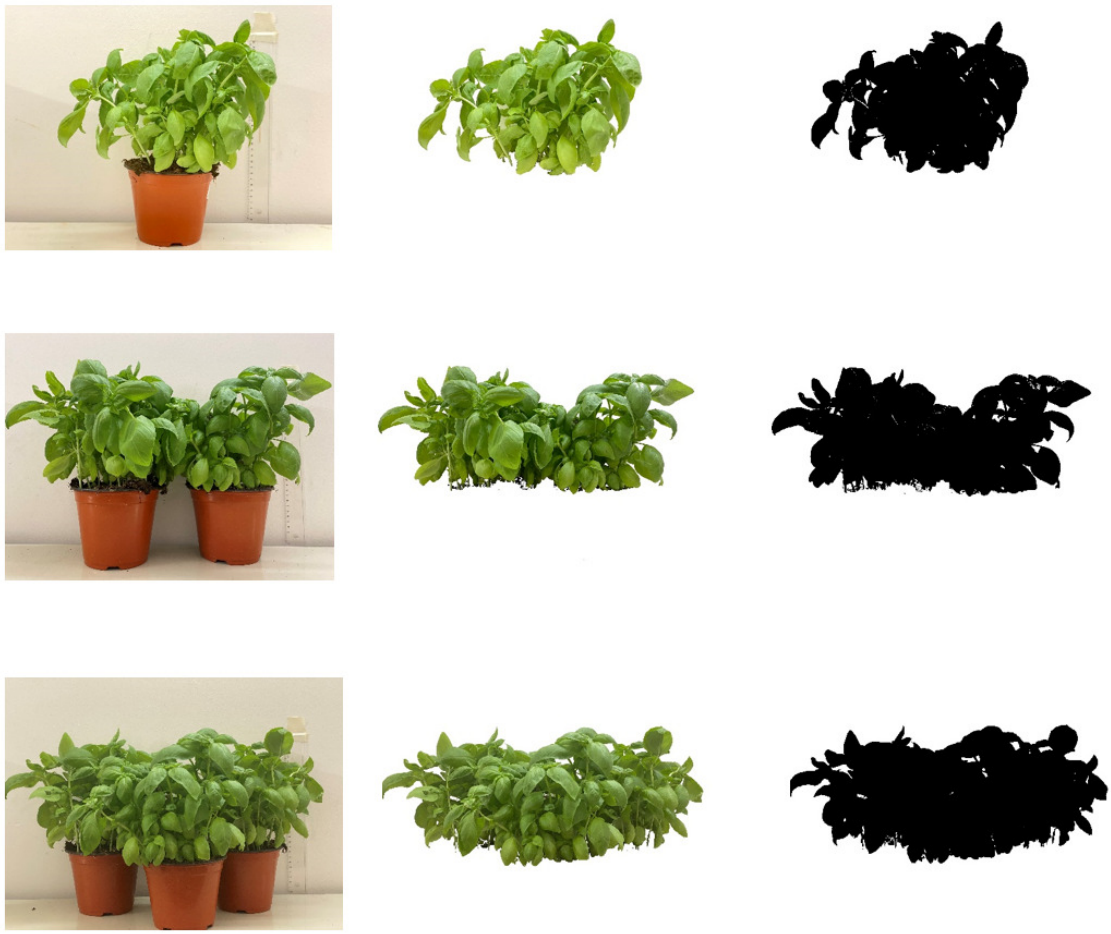

Figure 3.3: Example of image elaboration process for different set of Basil crops.

These images were subsequently processed and a calibration procedure was performed to establish the image size, followed by setting a color threshold to differentiate the crop from the background. This is essential for maintaining consistency across all images, thus allowing for a reliable comparative analysis. Non-target noise pixels were removed to enhance the accuracy of the analysis, as these extraneous pixels can significantly skew the quantification of porosity. Meanwhile, the crop itself was extracted. The resulting image

was then converted into a binary image, separating it into two distinct regions: a black area representing the crops and a white area representing the pores within the crops (see Figure 3.3 and Figure 3.4). This binary conversion simplifies the complex structures of the crops into a more analyzable form, making it possible to precisely calculate the porosity. This binary representation facilitated the assessment of porosity by quantifying the ratio of white area (pores) to the total area of the image. Through this method, this approach provides a clear and quantifiable measure of the porous nature of the crops, which is a key factor in understanding their aerodynamic behavior.

Figure 3.4: Example of image elaboration process for different set of Mentuccia crops.

3.3 Results and Discussion

3.3.1 Leaf area density assessment

Leaf area density was calculated as the ratio between leaf area per unit of vertical surface area and the sample thickness in the flow direction. This calculation involved a novel image elaboration technique, where the leaf area was determined from the binary image that differentiates between the crop leaves area and the pores within the crop. This technique not only enhances the precision of the measurement but also provides a more detailed understanding of the spatial distribution of the leaf area.

For the Basil crop, the LAD measurements varied with the number of pots inside the test chamber, indicating a direct relationship between plant density and leaf area distribution. This variation is a crucial finding as it suggests that LAD is sensitive to changes in crop density, a factor that could significantly influence airflow dynamics through the vegetation. With a single pot, the LAD was 2.41 m² m^{-3}. This value increased to 3.07 m².m^{-3} with two pots and further increased to 5.08 m² m^{-3} with three pots, as shown in Table 3.1. These gradual increases highlight the cumulative effect of adding more vegetation to the flow path, providing insights into how crop density affects aerodynamic parameters.

In contrast, Mentuccia crop demonstrated a different pattern in LAD values. For one pot, the LAD was relatively low at 1.17 m² m^{-3}, reflecting its less dense leaf arrangement. The increase in the number of pots to two and three resulted in LAD values of 1.64 m² m^{-3} and 1.93 m² m^{-3}, respectively. Although these increases were noticeable, they were less significant than those of Basil, indicating a different interaction pattern of Mentuccia with airflow, possibly due to its unique plant morphology.

Table 3.1: LAD for Basil and Mentuccia. Test 1 represents the case with 1 pot, Test 2 represents the case with 2 pots, and Test 3 represents the case with 3 pots.

Crop	LAD (m^2m^{-3})		
	Test 1	Test 2	Test 3
Basil	2.41	3.07	5.08
Mentuccia	1.17	1.64	1.93

3.3.2 Drag coefficient

The experimental studies on Basil and Mentuccia crops conducted in the wind tunnel, focused on the relationship between plant morphology, canopy density, and drag coefficient under varying air velocities. Initially, the tests focused on understanding how the frontal area and canopy size affect the drag coefficient. This is a critical point of study as it emphasizes how physical characteristics of crops interact with airflow dynamics.

Analyzing velocity and pressure drop data, the drag coefficient for each crop was calculated for different wind speed values ranging from 0.25 to 1 ms^{-1}, as indicated in Figure 3.5. For the Basil crop, the drag coefficient increased from 0.03 to 0.45, while for the Mentuccia crop, it ranged from 0.10 to 0.75. The observed increase in the drag coefficient with air velocity highlights the dynamic nature of plant-aerodynamic interactions. This increase of the drag coefficient with the air velocity was higher in Mentuccia because of the leaf arrangement and stronger branches, which do not bend as easily as the branches of Basil.

A critical aspect noted was the impact of canopy porosity on the drag coefficient. This finding is important as it stresses the influence of canopy structure on airflow resistance. For both crops, a more dense canopy resulted in a higher drag coefficient, indicating more resistance to airflow. Specifically, in Basil, the drag coefficient is on average about 0.26

for one crop, 0.36 for two crops, and 0.78 for three crops, with the highest pressure drop at 3.14 Pa. These values demonstrate a clear correlation between increasing plant density and aerodynamic resistance. On the contrary, Mentuccia showed a smaller increase, with the drag coefficient increasing from 0.48 for one pot to 0.57 for three pots. This difference must be attribute to the low canopy density of the Mentuccia crops. This difference must be attributed to the lower canopy density of the Mentuccia crops, highlighting how species-specific characteristics can affect airflow.

The flexibility of the plants also played a significant role in their aerodynamic behavior. In the wind tunnel, Basil leaves and branches bent and aligned with the airflow direction for the higher air velocities. This adaptability of Basil to airflow can have important implications for understanding how plants with similar characteristics behave in natural wind conditions. On the other hand, Mentuccia crops have a more rigid structure and therefore a greater obstacle to airflow. The firm structure of Mentuccia implies a strong ability to impact the airflow patterns in its surrounding area. The variation in drag coefficient between the initial and rotated crop tests highlighted these differences. While Mentuccia showed minimal change in drag coefficient upon rotation due to its firmer morphology, Basil demonstrated significant variations due to its flexible leaves changing orientation. This contrast in behavior between the two crops is crucial for modeling how different plant types affect airflow in diverse environmental contexts. The least difference in drag coefficient with ΔP was observed for both crops for the one pot configuration and for the lower velocities. However, this difference became more noticeable with an increased number of pots. For instance, with three pots of Basil, the difference reached approximately 0.18 between the normal and rotated canopy, while in Mentuccia, it was around 0.04, in-

dicating that rotation impacts the drag coefficient less in crops with smaller leaves and a more firmed morphology.

These variations in drag coefficient due to crop rotation provide valuable insights into the influence of plant orientation on airflow, a factor that can be crucial in wind-sensitive agricultural and urban planning designs. These results confirm as the drag coefficient is strongly related to the crop species and can not be considered constant with the air velocity. This finding is crucial as it challenges the traditional assumption of a uniform drag coefficient across different plant types and wind conditions. This result confirms the need for an appropriate choice and calibration of the drag coefficient before carrying out a CFD analysis and obviously this choice must be consistent with the fluid dynamic pattern and the expected air velocity around the crops. Consequently, achieving this will lead to accurate and reliable outcomes in CFD simulations, particularly in applications involving complex environmental interactions.

3.4 Conclusions

This study has provided valuable insights into the aerodynamic behaviors of Basil and Mentuccia crops, particularly in relation to leaf area density (LAD) and its impact on drag coefficient. The results indicate that variations in LAD are crucial in understanding how different plant structures interact with airflow. Specifically, Basil, with its higher and rapidly increasing LAD, showcased greater flexibility and a lower drag coefficient in the single pot test. This indicates that the denser and more flexible canopy is easier to adapt to airflow change.

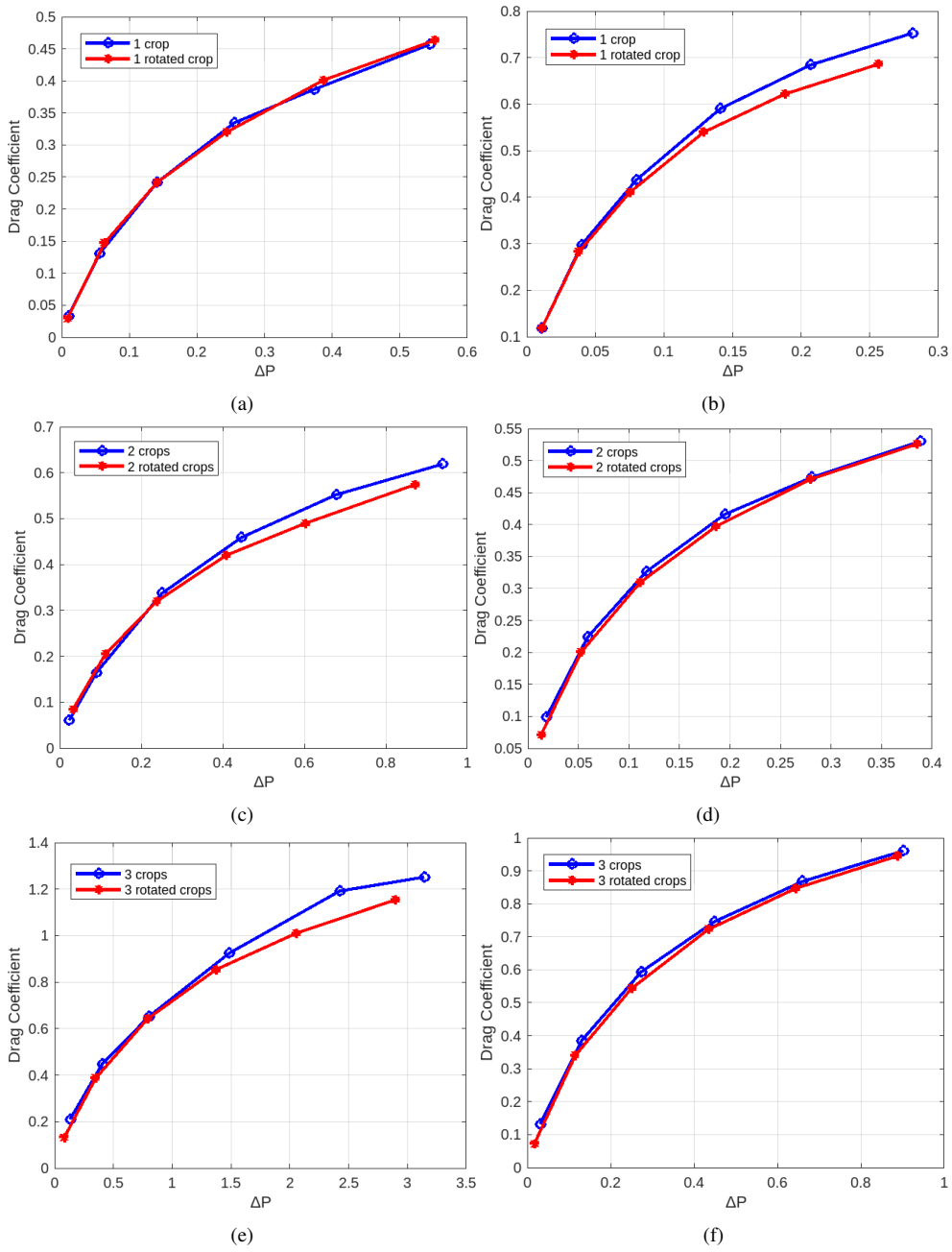

Figure 3.5: pressure drop versus drag coefficient for the frontal and 90° rotated side for Basil and Mentuccia crops with different count of pots inside the test chamber (a) 1 pot of Basil, (b) 1 pot of Mentuccia, (c) 2 pots of Basil, (d) 2 pots of Mentuccia, (e) 3 pots of Basil, (f) 3 pots of Mentuccia

In contrast, Mentuccia, characterized by its lower and more gradual LAD increase, demonstrated a different aerodynamic interaction. Since Mentuccia has stronger branches and more open canopy structure, minimal changes have occurred in the drag coefficient upon rotation, demonstrating its firmer morphology.

The results highlight the importance of analyzing wind velocity effects, where the drag coefficient increases with wind velocity for both crops, but the rate of increase varies due to morphological differences. For Basil, the drag coefficient increases with higher velocities, indicating its flexibility and the larger surface area exposed to airflow. Mentuccia shows more consistent increase, due to its stronger branches and less flexible leaves, which offer consistent resistance. The study also highlights that the drag coefficient is not solely determined by flow conditions and leaf density. The physical properties of the plants, including leaf flexibility and branch strength, play a significant role in their aerodynamic responses. This knowledge is critical for agricultural practices, as it assists in optimizing crop arrangements to minimize wind-induced stress while maximizing photosynthetic efficiency. Furthermore, It was noted that a higher density in the canopy is associated with an increased drag coefficient, and the changes in the morphology of the crop can have a significant impact on CD. In addition, this study highlights the potential applications of aerodynamic principles in precision agriculture. By integrating data on leaf area density and drag coefficients into agricultural planning tools, agriculturalists and agronomists could make more informed decisions about crop placement, spacing, and even cultivation techniques. For example, farmers can choose plant varieties with morphology that is naturally more resistant to wind damage, reducing the need for artificial supports.

However, the study faced limitations due to the experimental conditions. The exper-

iment was conducted during the summer's hot days, which led to rapid plant withering, challenging the maintenance of consistent leaf positions. Additionally, the small size of the test chamber limited the choices in crop species and canopy volume, which might impact the overall applicability of the results.

Chapter 4

Assessing urban microclimate impact: modeling the effects of vegetation and water bodies

4.1 Introduction

The ongoing escalation of urbanization and increasing population density in cities have increased the air and surface temperatures and the occurrence of summer heatwaves(Rogers *et al.*, 2019), resulted in Urban Heat Islands (UHIs) (Oke, 1982). This phenomenon not only escalates the energy demands of urban locales but also impacts the thermal comfort of individuals (Salata *et al.*, 2017), (Dong *et al.*, 2020). Urban heat islands are generally caused by less permeable surfaces, including buildings and paved roadways, replacing the vegetation of the surrounding rural areas, making the surface of cities rougher, less windy,

and frequently drier (Akbari and Pomerantz, 2001), (Stewart, 2011). The implementation and integration of green systems within the cities have been recognized as an effective countermeasure to mitigate UHIs, with a particular focus on augmenting the cooling effect (Qi and He, 2023).

Among the various green infrastructure approaches, the water bodies and tree canopies have an important role due to their capacity to generate significant cooling effects and support the establishment of a sustainable urban ecosystem (Zuvela-Aloise *et al.*, 2016). Within this complex system, computational fluid dynamics (CFD) simulations have emerged as an important tool for accurately modeling various characteristics of the urban environment (Kato, 2018), and for the analysis and prediction of cooling impacts in urban environments (Stavrakakis *et al.*, 2023). CFD simulations can analyze the impact of trees cooling effect by coupling the porous media model and the radiation model (Hong and Lin, 2015).

Nevertheless, little is known regarding the effectiveness of integrating both blue and green infrastructure to enhance thermal comfort. Furthermore, the extent to which these combined measures must be implemented to significantly counteract the observed warming trend remains unclear. This study aims to assess the predictive precision of Computational Fluid Dynamics (CFD) in understanding the cooling impact within complex urban settings characterized by tree-integrated pond infrastructures during a hot summer day when the heat islands effects are expected to be most intensive.

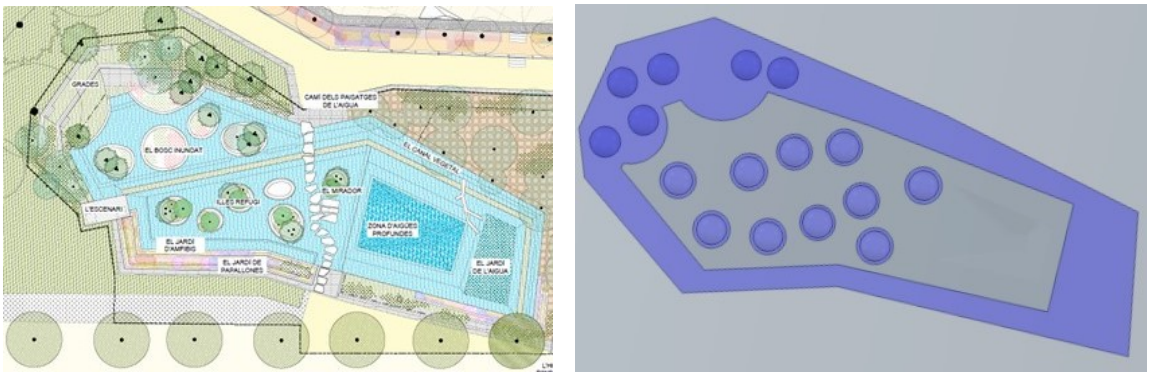

(a) Preliminary plan of the project (b) Simplified CAD model

Figure 4.1: Geometry of the case study

4.2 Materials and Method

4.2.1 Case study

This study investigates a naturalized pond in the central zone of Igualada, a municipality in the province of Barcelona. The pond is located in the central park between a residential area and an industrial area (41.588020 °N latitude, 1.623374 °E longitude) and covers an area of 512.47 m^2.

The pond has been structured into two connected sections: a deep-water area with a depth of 1.5 m and a shallow-water area where the water reaches a depth of 0.40 m. The latter serves as a habitat for tree zones designed to serve as a flooded forest environment; these zones are partially submerged into water with an approximate diameter of 1.5 m. These zones are formed by flexible gabions and a structured coconut fiber roll, and filled with a layer of gravel and topsoil to encourage the roots of the trees.

The tree species within the park includes Tamarix africana, with an average height of 4 m; Fraxinus angustifolia, reaching up to 5 m; Acer monspessulanum, with a height of 3 m;

Figure 4.2: Alnus glutinosa (i.e. *common alder*) in fully mature status.

and Alnus glutinosa (i.e. *common alder*), which typically grows to 4 m. For the purposes of this study, Alnus glutinosa (i.e. *common alder*) was selected for the simulation, since they are located in the shallow water area. Moreover, its morphological characteristics as shown in Figure 4.2, allow it to be represented as a cylindrical volume capped with a hemispherical crown within the computational model.

The pond is surrounded by diverse flowering shrubs to guarantee year-round flowering, and promoting biodiversity within the ecosystem. average shrubs height is 40 cm. Total water area is 404.77 m^2 while total vegetation area is 107.70 m^2.

The images in Figure 4.3 were obtained during the initial phase of implementing the project. Since this research aims to account for the system in its fully mature state, the

(a) deep water area

(b) shrubs surrounding the pond

(c) shallow water area

(d) tree zone in the shallow water area

Figure 4.3: Overview of the case study

porous media in the numerical simulation will represent fully grown trees, ensuring a comprehensive representation of the mature environmental conditions.

Igualada has a Mediterranean climate characterised by mild, relatively moist winters and warm, relatively arid summers. During the months of June, July, and August, Igualada experiences its warmest period, with average daily temperatures ranging between 21 and 24 °C throughout the day. In summer, temperatures peak at around 32°C, while the minimum temperature remains around 16°C. Alternatively, winter temperatures in Igualada rarely drop below 0°C, with the highest temperature recorded averaging around 17°C. For the purposes of the current study, climatic data are extracted from the weather station located in Òdena, 3 km far from the pond.

4.2.2 Governing Equations

This research implements wind simulations utilizing the standard *k*-ε model. This model has been significantly employed in simulating vegetation behavior and is chosen for its ability to achieve acceptable accuracy while maintaining reasonable computational efficiency. The derived time-averaged governing equations, describing energy, momentum, and mass for incompressible steady fluids, are shown in the following equations:

$$\frac{\partial \varphi}{\partial t} + \frac{\partial}{(\partial x_i)}(u_i \varphi) = \frac{\partial}{(\partial x_i)} \Gamma \varphi \frac{\partial \varphi}{\partial x_i} + S_\varphi \tag{4.1}$$

Where φ represents scalar quantities such as velocity u in m s^{-1}, turbulent kinetic energy k in $m^2 s^{-2}$, and turbulent dissipation rate ε in $m^2 s^{-2}$. The mean velocity vector is represented by u; Γ_φ is the effective diffusion coefficient for each variable, and S_φ is

the source term in equation. The standard k-ε model solves two equations, one for the turbulent kinetic energy (k) Eq.(4.2), and the other is the energy dissipation rate (ε) Eq. (4.3).

$$k = \frac{u_*^2}{\sqrt{C_\mu}}\left(1 - \frac{z}{\delta}\right) \tag{4.2}$$

$$\varepsilon = \frac{u_*^2}{kz}\left(1 - \frac{z}{\delta}\right) \tag{4.3}$$

where δ refers to the depth of atmospheric boundary layer and C_μ represents the the eddy viscosity coefficient in k-ε models and it was set to = 0.09.

The presence of trees and shrubs affect the airflow by behaving as a porous media. In general, the influence of vegetation on airflow and turbulence is expressed through a decrease in wind speed and an increase of turbulence within the volume defined by the vegetation. In this research, the trees and shrubs are defined as a volume of air subjected to specific conditions. The effects of trees and shrubs are considered by including source terms into the computational fluid dynamics (CFD) model following Darcy-Forchheimer equation;

$$\mathrm{S} = -\,\rho_\mathrm{a}\,\mathrm{LAD}\,\mathrm{C_D}\mathrm{V}^2 \tag{4.4}$$

where ρ_a is the air density (kg m^{-3}), LAD is the leaf area density (m^2 m^{-3}),V is the air velocity, and C_D is the dimensionless drag coefficient. For this study, LAD (0.85 m^2 m^{-3}) and C_D (0.6) were derived from (Mochida *et al.*, 2006).

Beside their impact on the flow dynamics, trees have a significant influence on the over-

all energy balance. The vegetation was partitioned into elementary volumes, and within each of these volumes, the transfers of heat and water vapor mass were simulated through sink or source terms. A radiative flux is allocated to each elementary volume, undergoing conversion into sensible and latent heat. Expressing the energy balance mathematically, it can be formulated as follows:

$$G_a = Q_s + Q_l \tag{4.5}$$

where G_a (W m^{-3}) is the radiative flux absorbed by each cell in the porous media, Q_l (W m^{-3}) is the latent heat flux density represents the transpiration process, Q_s (W m^{-3}) is the sensible heat flux density and represents the transfer of sensible heat between the trees and the ambient air. The exchange of sensible heat flux between the canopy and the ambient air is subject to the temperature difference between the leaves and the surrounding air, in addition to the leaf density. The governing dynamics are described by the following equation:

$$Q_s = LAD\ \rho_a\ C_p\ (T_l - T_a)\ /r_a \tag{4.6}$$

In the equation, C_p is the specific heat of air under constant pressure (J $kg^{-1}\ k^{-1}$), while r_a represents the leaf's aerodynamic resistance (s m^{-1}). T_l and T_a refer to the temperatures of the leaves and the surrounding air within each cell, respectively. Additionally, this equation assumes uniform temperatures on both sides of the leaf.

The latent heat flux, defined as the transpiration rate, was derived with respect to the difference in air humidity. This difference represents the saturated water content of the air at canopy temperature w_L (kg kg^{-1}), and the specific humidity of the air w_a (kg kg^{-1}):

$$Q_l = \lambda LAD\rho_a \frac{(w_L - w_a)}{(r_a + R_s)} \tag{4.7}$$

where λ is the latent heat of water vaporization (kJ kg^{-1}), and R_s is the leaves stomatal resistance (s m^{-1}). In this research, the stomatal resistance was set to a constant value of 100 (s m^{-1}) following (Li *et al.*, 2023).

Radiative transfer modeling includes solar radiation. In this research, global solar contribution is calculated as the total of the direct, diffuse, and reflected irradiances. In order to simplify the model and enhance computed velocity and precision, heat conduction and the latent heat of vaporization from the underlying surface are both neglected. The water thermal interaction consists of the emission of radiant heat to the surroundings and heat transfer through convection with the air. Moreover, this study excludes the thermal transmission process between water and soil in the pond.

4.2.3 CFD model

For the assessment of urban microclimates, the numerical model employed in this study utilizes the finite volume method implemented in the STAR-CCM+ software to simulate the complex fluid dynamics. Governing equations, including the Navier-Stokes equations for airflow, the energy equation, and the turbulence model, are discretized over the computational domain through a structured grid.

A computational model was developed for the vegetation and the pond. The vegetation was represented as a source term within the CFD, considering it as a porous medium. The tree's shape is simplified as a cylinder topped with a hemisphere, which provides model-

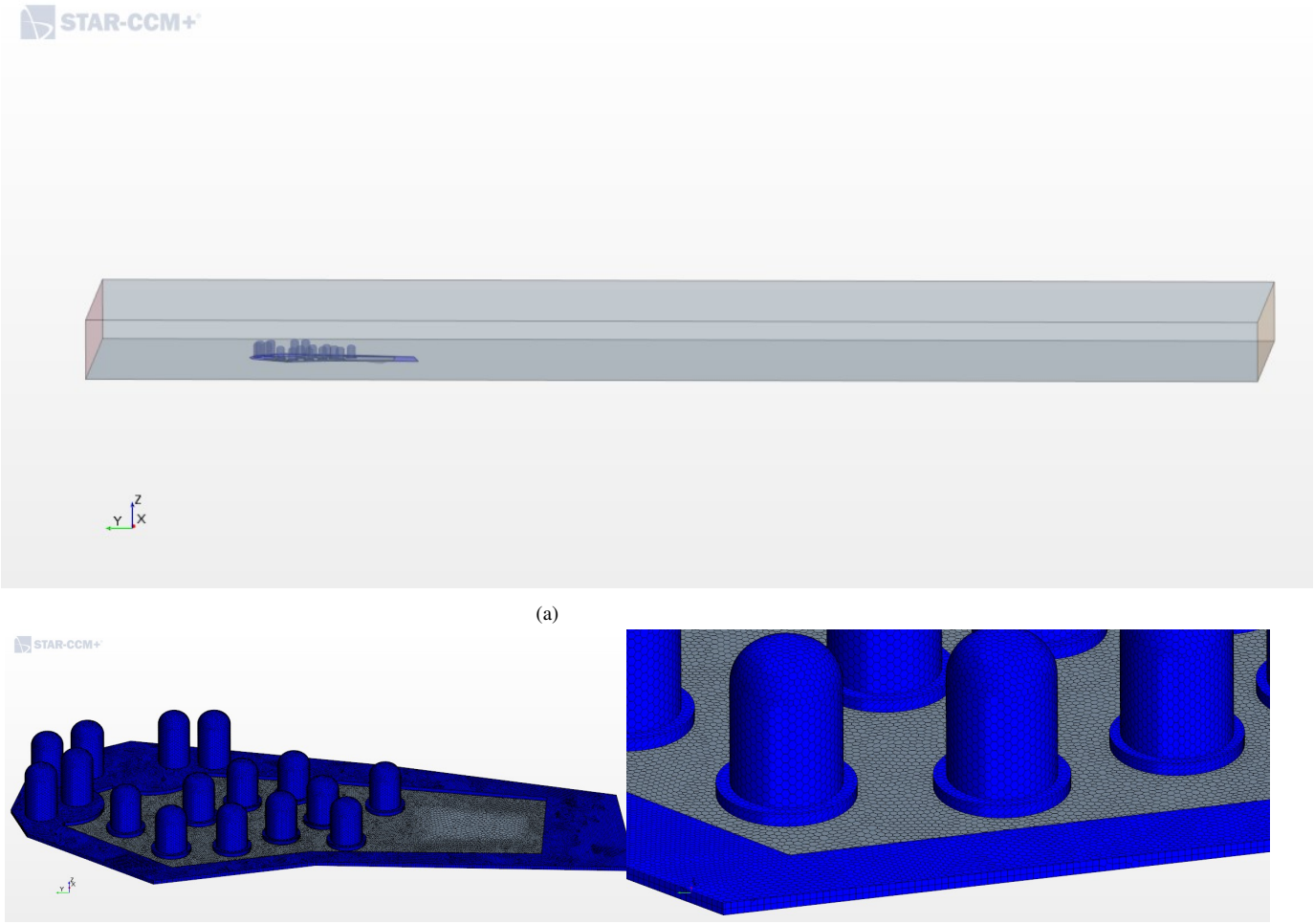

(a)

(b) (c)

Figure 4.4: (a) Computational domain used for the CFD simulation. (b) View of the polyhedral mesh of the study case. (c) Detail of the mesh close to a tree

ing advantages, computational efficiency, and convergence benefits, while approximately simulating the tree's actual shape. The trees in the shallow part of the water and the trees in the soil around the lake have 4 m and 5 m heights, respectively. The water pond was characterized by considering surface radiation, with energy exchange between the water and the surrounding air through convection and surface radiation. Additionally, the surface of a water pond is characterized by setting boundary conditions for surface temperature and humidity. The water surface is considered as an isothermal wall, acting as a heat sink due to evaporation.

The computational domain has a length of 394.8 m and a width of 135 m, with a height of 20 m, including the pond, trees, and shrubs. A view of the domain adopted in the simulations is reported in Figure 4.4a. A polyhedral mesh was selected to minimize numerical errors and simplify the calculation convergence, with a refined mesh specifically applied around trees, shrubs, and sharp edges, as illustrated in Figure 4.4b and 4.4c.

A steady-state simulation was conducted, utilizing the ambient temperature at 12:00 a.m. on August 1st in Igualada, obtained from the weather station (Òdena). In order to evaluate thermal impacts, the natural convection module was activated, employing an incompressible real gas model for air density. Radiation exchanges were assessed through the S2S radiation model, by activating a geometric function known as a "view factor" for energy exchange parameters. Solar Ray Tracing in the Solar Load Model, available in Star-CCM+ software, was also activated to account for the solar radiation, which is determined based on the direction of the solar beam relative to the specified date and geographical coordinates. Additionally, the model incorporates an option to adjust for cloudiness. In this case, the cloudiness factor is set to 1, following clear sky conditions in line with the

meteorological information obtained from weather stations.

For the airflow model, a logarithmic law profile, derived from meteorological conditions and surface roughness, was applied as the boundary condition at the inlet opening. Wall boundary conditions were enforced on the top side (sky) and lateral sides of the computational domain, while an atmospheric pressure-outlet condition was imposed at the exit (right side).

All parameters and boundaries were established using User Defined Functions (UDF) coupled with Star-CCM+ software. The inlet air temperature (Ta) was provided by the Weather Station. The inlet velocity profile is represented through Equation (4.8):

$$U\left(z\right) = \frac{u_*}{K} ln\left(\frac{z + z_0}{z_0}\right) \tag{4.8}$$

Where: U(z) is the horizontal velocity in z direction (m s^{-1}), u_* is the friction wind velocity, K = 0.35 is the von Karman's constant, z = 10 m is the height above the ground and z_0 is surface roughness. The modeling approach is general and can be applied to any urban environment, as it includes universal physical models within the simulation, making it adaptable and replicable.

4.3 Results and discussion

Considering the aim of investigating the integrated cooling effects, the study will take into consideration two different case scenarios. The first case scenario will involve a simulation that represents both trees and a water body, thereby providing results of their combined impact on cooling. The second case scenario, will focus exclusively on simulating the

presence of trees without the water. This approach is set up to facilitate a direct comparison between the two scenarios, allowing for a better understanding of the individual and combined contributions of trees and water bodies to the overall cooling effect.

The analysis of both cases, will be conducted under two different inlet air velocities 3.3 m.s^{-1}, and 1 m.s^{-1}, to understand how varying air velocities influence the cooling efficiency of each system.

4.3.1 Cooling effect

Figure 4.5 indicates the simulated surface temperatures to show the difference in the range of cooling air temperature between the integrated system and the only trees system; the combination of trees and a water body is more efficient in cooling than trees with soil ground, where the average reduction in temperature was (1.5 °C) and (0.5 °C), respectively. The evaporative cooling from the water body, combined with the shading and transpiration from trees, results in a more substantial reduction in temperatures.

The analysis of temperature distribution across different sections of both systems reveals interesting results, as illustrated in Figure 4.6. In the cross-sectional area that passes through the shallow water zone, the temperature profiles for both the case with trees and water, and the one with only trees, display a different temperature profile. While the trees impact the temperature of the airflow in both cases, their cooling effect is significantly increase in the presence of water. This indicates that the integration between trees and water has more impact on the overall cooling efficiency.

This impact is further noticed in the cross-sectional area of the deep water zone, see figure 4.7. Here, the cooling effect of water becomes notably significant in comparison to

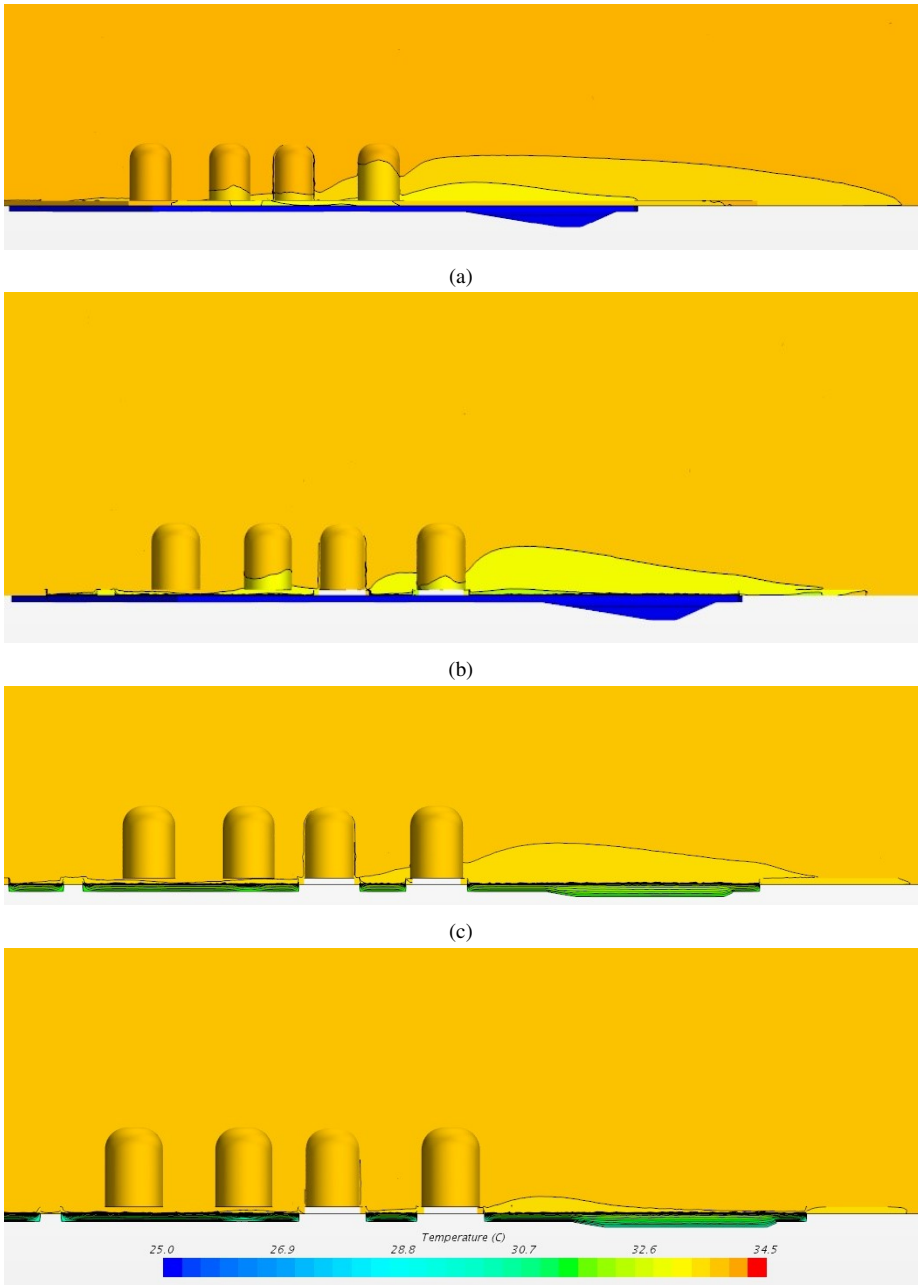

Figure 4.5: Comparative analysis of temperature distribution in long sectional view at different scenarios: a) Trees and water at 1 m/s inlet velocity, b) Trees and water at 3.3 m/s inlet velocity, c) Trees only at 1 m/s inlet velocity, d) Trees only at 3.3 m/s inlet velocity

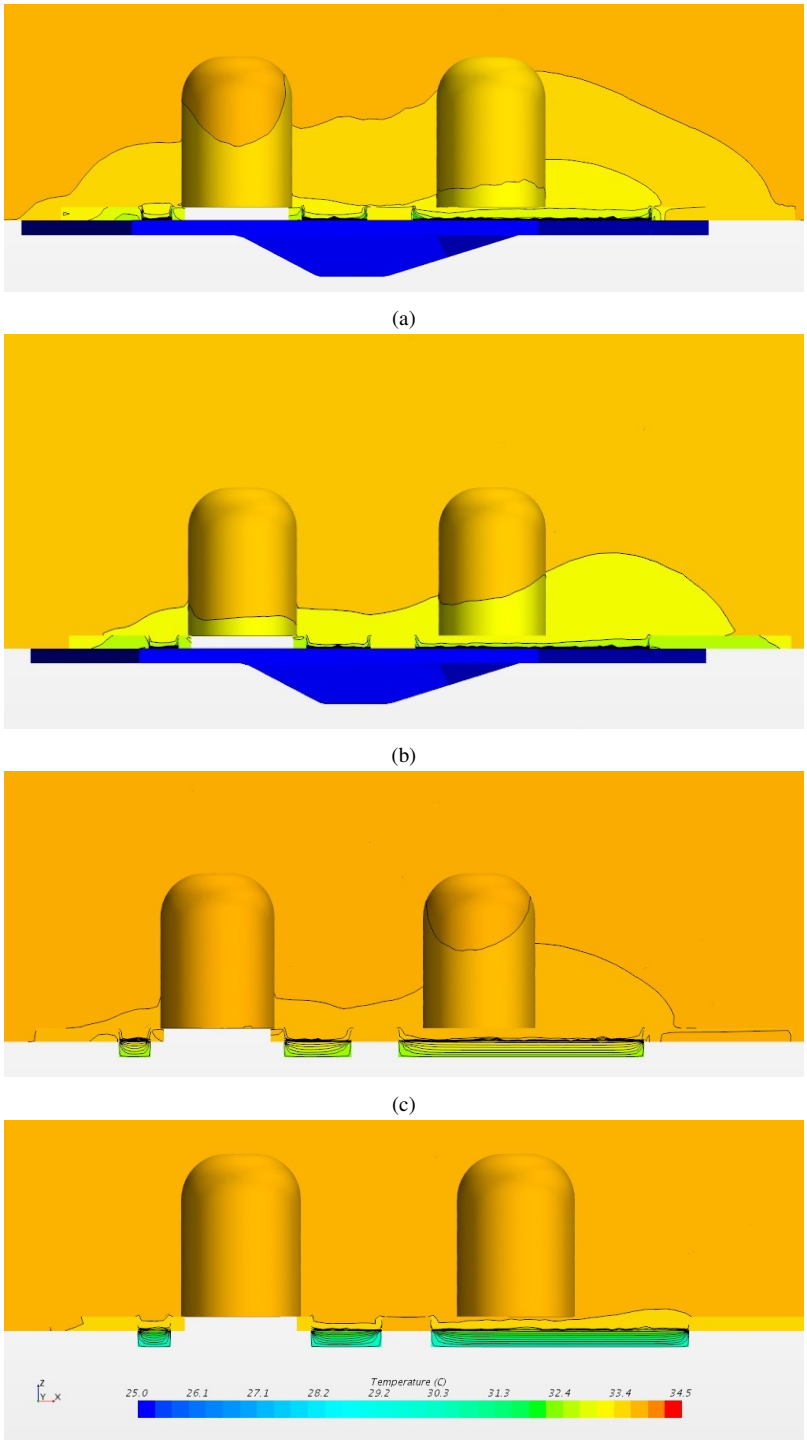

(a)

(b)

(c)

(d)

Figure 4.6: Comparative analysis of temperature distribution in a cross sectional view in the shallow water area at different scenarios: a) Trees and water at 1 m/s inlet velocity, b) Trees and water at 3.3 m/s inlet velocity, c) Trees only at 1 m/s inlet velocity, d) Trees only at 3.3 m/s inlet velocity

the scenario without water, the cooler temperature of a water body creates a greater temperature differential between the air and the surface of the water, enhancing the convective heat transfer. For example, in figure 4.7, the airflow already passed through the trees area in both cases, but in the case without water the reduction in temperature is barely noticeable. This difference illustrates that the presence of water plays a dominant role in influencing the temperature within these areas.

4.3.2 Wind velocity

The cooling effect of the water body is highly dependent on wind boundary conditions. This dependency is crucial, despite the fact that wind direction has not been addressed in this analysis. The extent of the area influenced by the water body, along with the intensity of its cooling effect, varies significantly with changes in wind velocity. Specifically, the maximum observed temperature difference near the water body happened when the velocity is (1 m s^{-1}). Figure 4.8 and figure 4.9, present a comparative analysis of air velocities along the domain for scenarios with and without the water. Notably, the cooling effects of both cases are observed up to a distance of 100 m downwind.

Similarly, the airflow velocity impacts the cooling effect of trees, particularly in the leeward area. It is observed that air temperature within this zone increases with the increasing wind velocity. Notably, when the wind velocity is 3 m s^{-1}, the cooling effect of the trees decreased on their leeward sides. However, the spatial range of the tree's influence on air temperature is broader under conditions of higher wind speed (3 m s^{-1}) compared to scenarios with lower wind speeds (1 m s^{-1}).

An interesting spatial dynamic is noted with the change in wind speed, the influence

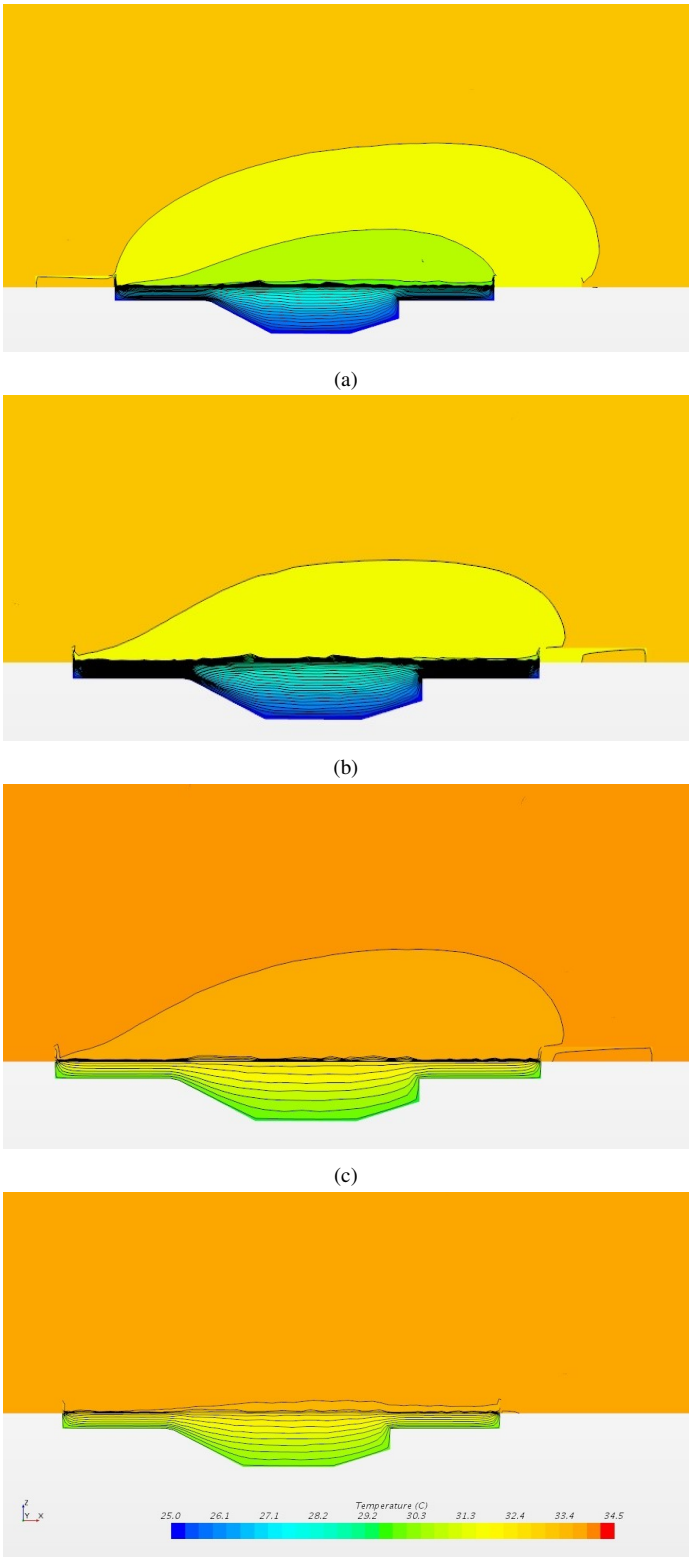

(a)

(b)

(c)

(d)

Figure 4.7: Comparative analysis of temperature distribution in cross sectional view at deep water part in different scenarios: a) Trees and Water at 1 m/s Inlet Velocity, b) Trees and Water at 3.3 m/s Inlet Velocity, c) Trees Only at 1 m/s Inlet Velocity, d) Trees Only at 3.3 m/s Inlet Velocity

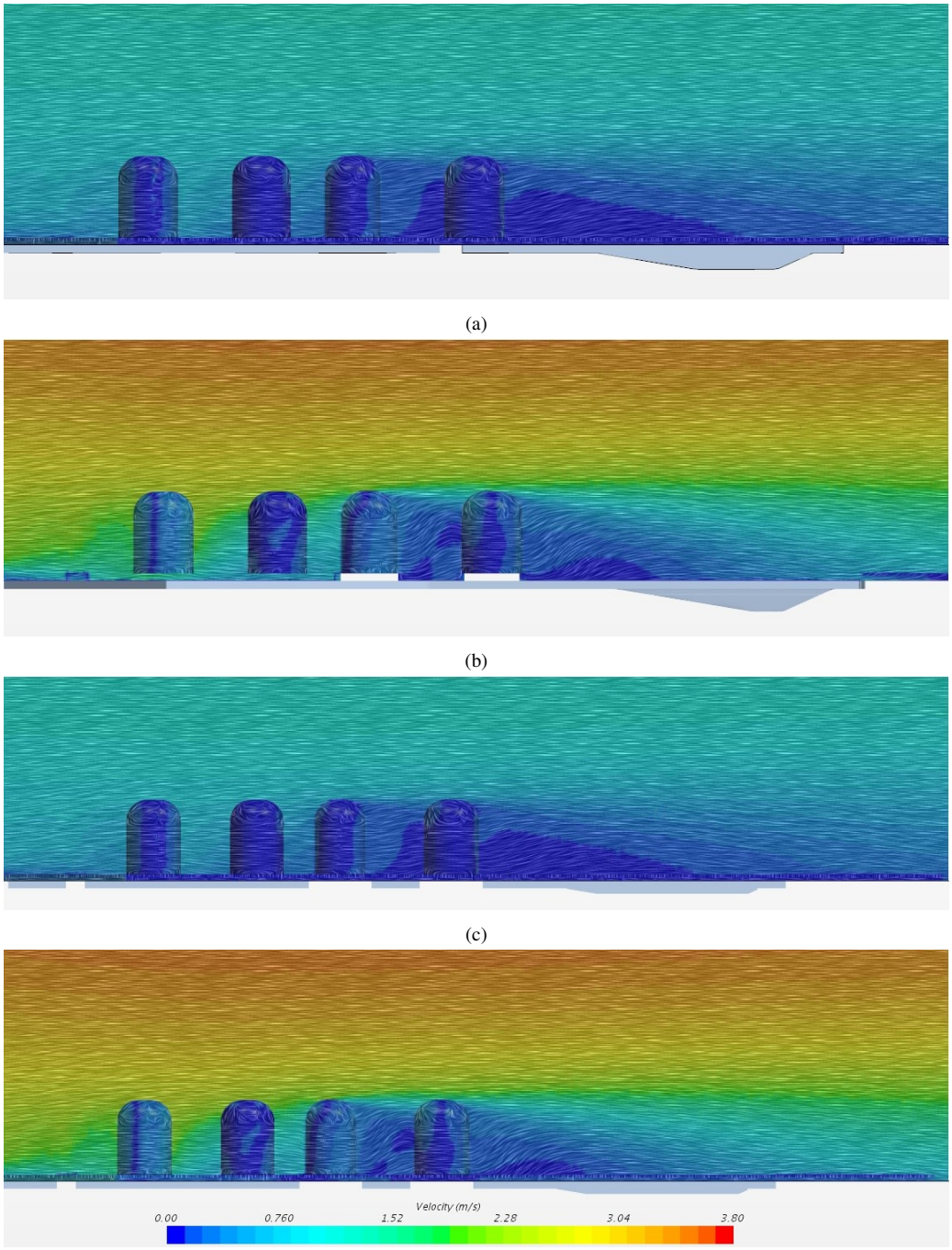

(a)

(b)

(c)

(d)

Figure 4.8: Comparative analysis of velocity distribution in different scenarios: a) Trees and water at 1 m/s inlet velocity, b) Trees and water at 3.3 m/s inlet velocity, c) Trees only at 1 m/s inlet velocity, d) Trees only at 3.3 m/s inlet velocity

range of the tree adopts a "long and narrow" configuration. This change in the tree's impact zone highlights the complex relationship between wind speed and the drag force imposed by the porous trees which leads to modify local air temperatures. Similar results obtained by (Morakinyo *et al.*, 2016) through simulation that areas covered with trees experienced a reduction in wind speed up to 50%, in contrast to areas without trees.

To evaluate the impact of different scenarios on pedestrian thermal comfort, results were taken from 17 points distributed randomly across the simulated area. These results were collected from both cases: the trees and water pond, and the other with only trees. Each case was assessed under two wind conditions 1 m s^{-1} and 3.3 m s^{-1}. To approximate average human height, data were collected at two elevations: 1 m and 2 m, based on the standard height of 1.75 m suggested by (Kang *et al.*, 2020), (Tseliou *et al.*, 2023).

The results, shown in figure 4.10, with the highlighted area represent the presence of water in one case and the ground surface in the other. For the lower wind velocity condition (1 m s^{-1}), there was a notable variation in air movement between the two scenarios. Specifically, the wind velocity at 1 m height ranged from 0.06 m s^{-1} to 0.11 m s^{-1} in the trees-only scenario, Figure 4.10 (a), significantly lower than the 0.06 m s^{-1} to 0.56 m s^{-1} recorded in the presence of a water body, Figure 4.10 (b). Particularly, Point 9, shielded by a tree, showed consistent velocity across both scenarios. Points 7 and 8, however, demonstrated enhanced air velocity in the water pond scenario, with velocities of 0.51 m s^{-1} and 0.56 m s^{-1} respectively, compared to only 0.01 m s^{-1} and 0.07 m s^{-1} in the trees-only scenario. This suggests that water bodies may substantially improve air circulation near the ground level under mild wind conditions. At the 2 m elevation, the velocities were similar in both scenarios, with the largest variance being ± 0.08 m s^{-1} at Point 8, indicating

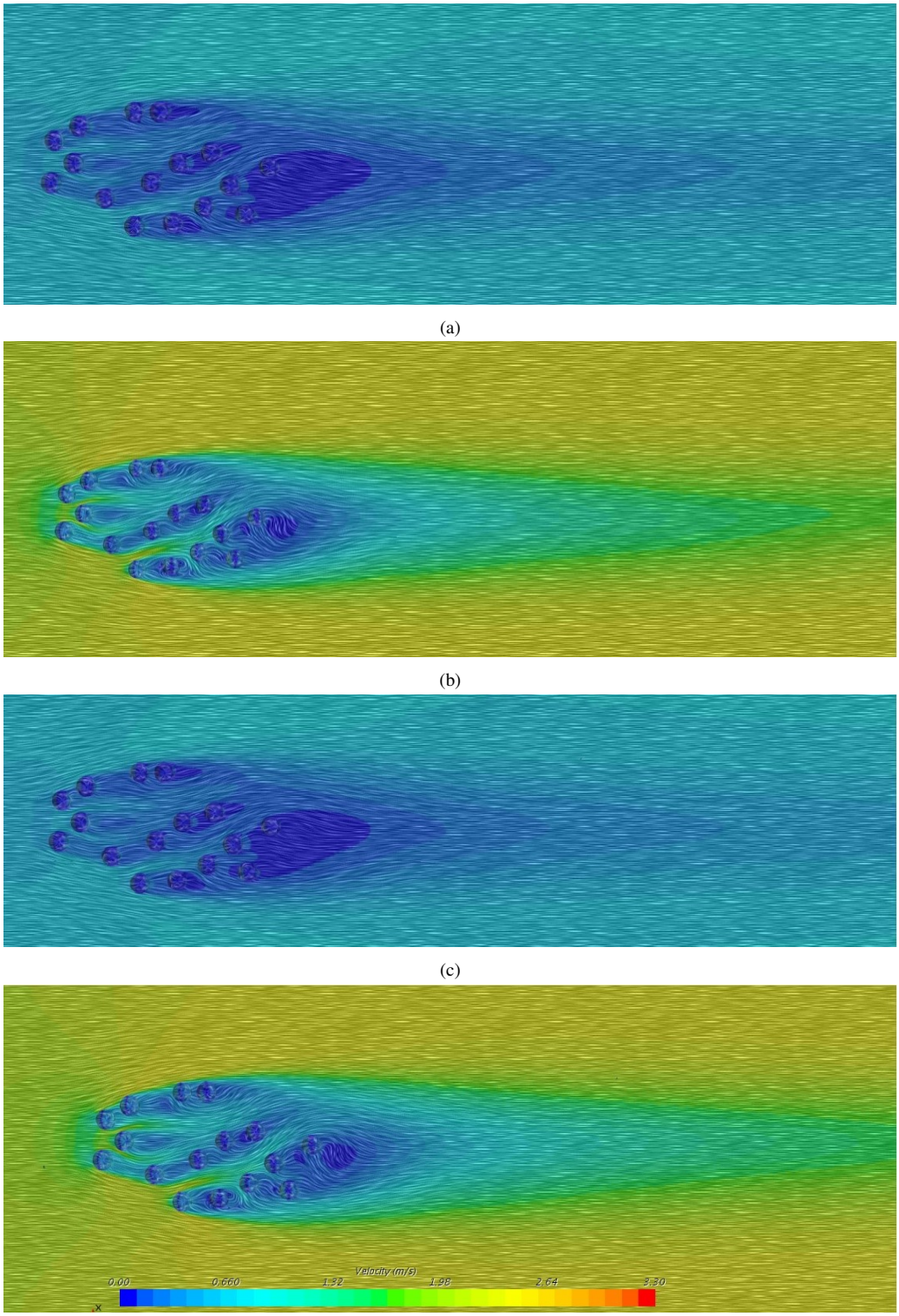

(a)

(b)

(c)

(d)

Figure 4.9: Top view shows the velocity distribution at 1.7m height a) Trees and water at 1 m/s inlet velocity, b) Trees and water at 3.3 m/s inlet velocity, c) Trees only at 1 m/s inlet velocity, d) Trees only at 3.3 m/s inlet velocity

that the influence of the water diminishes at higher elevations.

Under the stronger wind condition of 3.3 m s^{-1}, a higher difference was observed. Without water, Figure 4.10 (c), the velocity at 1 m height varied from 0.39 m s^{-1} to 0.77 m s^{-1}, significantly lower than the 0.35 m s^{-1} to 1.83 m s^{-1} range observed with water, Figure 4.10 (d), with Point 7 recording the highest velocity of 1.83 m s^{-1}. At 2 m, both scenarios showed increased velocities compared to the 1 m s^{-1} wind condition, with values reaching up to 2.37 m s^{-1} with the presence of water at Point 7, slightly higher than the 2.3 m s^{-1} observed in the trees-only scenario. This enhanced wind velocity near water can be attributed to the smooth surface of the water pond, which reduces surface friction and allows smoother airflow.

The results also indicate a minimal change in wind velocity between the two cases in the trees area that surround the water pond at both heights of 1 m and 2 m, suggesting a limited influence of the immediate vicinity on local wind speeds at these heights. This observation was consistent across scenarios with and without the addition of water bodies, indicating that the micro climatic impact at pedestrian level might be constrained by the trees which can act as wind buffers.

The highest differences in wind velocity in surrounding area between the two cases, was 0.08 m s^{-1} at 1 m and 0.09 m s^{-1} at 2 m in low wind conditions (1 m s^{-1}), and even less under higher wind conditions (3.3 m s^{-1}), imply that the surrounding trees provide a shielding effect which reduces wind penetration at lower levels. (Kumar *et al.*, 2013) supports this, noting that roughness elements like trees and small structures around water bodies can introduce additional turbulence, which significantly affects the convective mass transfer at lower elevations, thus impacting the local microclimate.

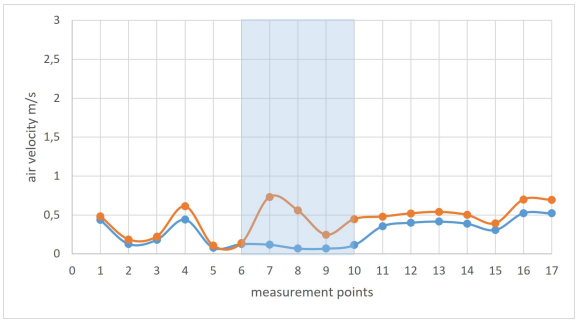

(a)

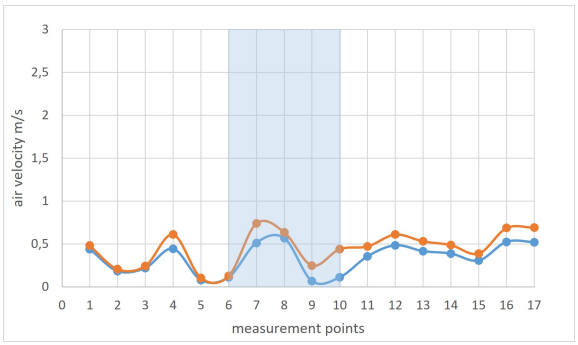

(b)

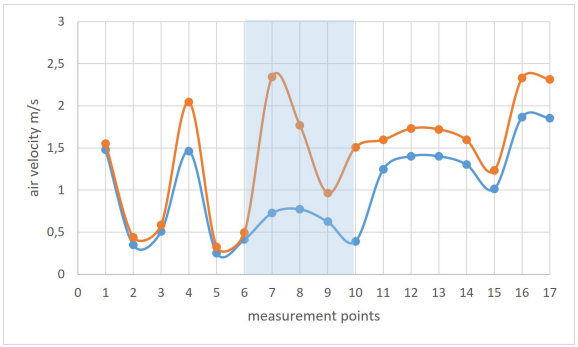

(c)

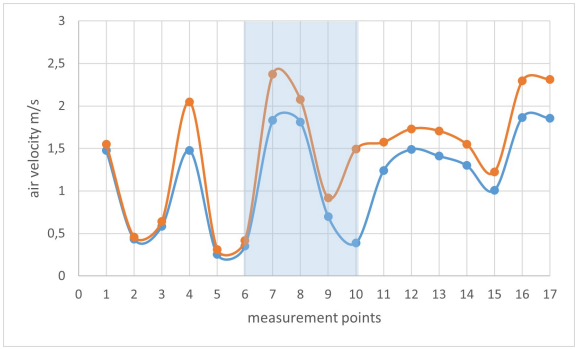

(d)

Figure 4.10: Comparative analysis of wind velocity at two heights. (a) input air velocity of 1 m/s in the trees-only case, (b) input air velocity of 1 m/s in trees and water pond case, (c) input air velocity of 3.3 m/s in the trees-only case, (d) input air velocity of 3.3 m/s in trees and water pond case

These results recommend the strategic placement of such natural elements in urban planning to enhance pedestrian comfort and mitigate urban heat. The findings can guide policymakers in promoting green infrastructure, contributing to healthier, more sustainable urban environments.

4.4 Conclusion

This study successfully utilized computational fluid dynamics (CFD) to assess the predictive accuracy in understanding the cooling effects within complex urban landscapes, particularly the integration of trees and water systems, during peak heat island conditions on a hot summer day in Igualada, Barcelona.

The findings indicate that the combination of trees and water bodies is more effective in cooling urban environments than trees with soil ground. The average temperature reductions observed were 1.5°C for the integrated trees-water system and 0.5°C for the only trees system. The increased cooling effect can be due to the interaction of evaporative cooling from water and the shading and transpiration effects of trees.

The intensity of the cooling effect varied with changes in wind velocity, with the maximum temperature difference observed at a wind velocity of 1 m s^{-1}. Additionally, the influence of trees on local air temperatures show significant spatial variations in response to changes in wind velocity. This indicates the relationship between wind velocity, the drag force generated by trees.

The study also highlights the significant role of water bodies in enhancing air circulation at pedestrian level under low wind conditions (1 m s^{-1}), where their smooth,

low-friction surface facilitates better airflow compared to areas with ground and trees. However, the influence of these water bodies diminishes at higher elevations and under stronger wind conditions, where trees begin to have a more dominant effect on modulating air flows. This is confirmed by the fact that trees act as natural buffers, maintaining more consistent wind speeds at both tested heights and significantly reducing penetration of high wind condition, enhancing pedestrian comfort. These findings can guide urban planning and design, influencing policies to integrate natural features for improved pedestrian comfort and environmental resilience.

However, it is important to acknowledge the limitations of the study. The absence of experimental measurements and the simplifications in CFD model make it difficult to quantitatively evaluate the performance of these simulations. Furthermore, the small reduction in heat observed, is related to the choice of the hottest day in August at mid-noon, and this highlights the need for comprehensive analysis across varied conditions.

Future work

To take this research further, future studies should focus on the following aspects:

- Experimental validation: Conducting field measurements to validate and refine the CFD model, enhancing its accuracy and reliability.
- Wind direction analysis: Including wind direction into the analysis to understand its full impact on the cooling effects of trees and water bodies.

- Seasonal and diurnal variations: Examining the cooling effects under different seasonal and diurnal conditions to have a bigger range of urban heat island phenomena.
- Comparative studies: Conducting comparative studies with different vegetation types and water body sizes to determine optimal configurations for maximum cooling efficiency.

Chapter 5

Conclusions and Summary

The aim of this thesis is to investigate the complex interactions between vegetation and its environment through varied settings, including indoor environments like greenhouses, outdoor environments like landscapes, and controlled environments like wind tunnels. In Chapter 1, a thorough review established the foundation for the study, highlighting current knowledge, motivations, and research goals.

Chapter 2 discussed the microclimatic conditions within a greenhouse, applying CFD to simulate crops as porous media. This approach provided significant insights into the heat and mass transfer processes between crops and air. The results from this chapter demonstrated the effectiveness of CFD in accurately modeling greenhouse environments, thereby enhancing our understanding of thermal exchanges in the establishment of more energy-efficient and productive greenhouses. Additionally, this chapter presented details regarding the influence of solar radiation on the thermal comfort of crops within the greenhouse environment, identifying the optimal conditions for crop growth and development.

Chapter 3 investigated the aerodynamic behaviors in Basil and Mentuccia crops, utilizing wind tunnel experiments to analyze their interaction with airflow. A crucial finding was the correlation between canopy density and the drag coefficient. It was observed that for both crops, a denser canopy significantly increased the drag coefficient, suggesting an increased resistance to airflow. This finding is important, as it emphasized the direct impact of canopy structure on the plant's aerodynamic profile.

Further, the study highlighted that variations in the leaf area density (LAD) were directly influenced by the number of pots within the test chamber. This correlation demonstrates a connection between plant density and the distribution of leaf area, and explains the relationship between physical plant characteristics and their aerodynamic responses. It was also noted that rotational adjustments or the changes in frontal area had a smaller impact on the drag coefficient in crops with smaller leaves and more rigid morphologies, such as Mentuccia. This aspect is particularly significant, as it suggests a degree of morphological adaptation in response to environmental forces, with potential implications for plant breeding and cultivation practices.

The research in this chapter contributes substantially to the understanding of plant aerodynamics, especially in relation to agricultural practices. The results obtained from the study of Basil and Mentuccia can inform strategic decisions in crop arrangement and selection, aimed at minimizing wind-induced stress and maximizing photosynthetic efficiency. For instance, the findings could guide the selection of crop varieties for specific environmental conditions, favoring those with aerodynamic properties that align with the dominant climatic challenges.

From a scientific perspective, these results contribute to a growing body of knowledge

in plant physiology and environmental interaction. The study contributes to future research investigating morphological adaptations of plants to aerodynamic stresses. Additionally, the integration of these aerodynamic considerations into computational models could enhance the precision of climate-smart agricultural strategies, leading to more sustainable and productive farming methods.

Chapter 4 introduced a CFD simulation method specifically designed to investigate the regulatory effects of trees and water body on outdoor microclimates under varying external conditions. The study approach not only examined the temperature and wind distribution in the presence of water but also compared these conditions to scenarios with no water, thereby highlighting the critical role of urban blue system.

The findings provide insights for urban design and engineering, particularly in the strategic layout of trees in urban areas. The research emphasizes the relationship between urban water bodies and tree presence, demonstrating how this combination can effectively reduce urban heat island (UHI) effects.

The outcomes of this research are highly relevant for urban planners. They offer data that support the cooling properties of water bodies, further improved by trees, to combat urban heat island effects. Such knowledge is crucial in developing urban spaces that are more livable, comfortable, and sustainable.

While this chapter focused on an open landscape distant from building structures, the results can contribute to future research. These investigations are expected to increase the knowledge of how urban green systems can be best utilized not only for aesthetic purposes but also for improving microclimatic conditions, thereby enhancing the overall quality of urban life.

Bibliography

Akbari, H. and M. Pomerantz, "Cool surfaces and shade trees to reduce energy use and improve air quality in urban areas", Solar Energy **70**, 295–310 (2001).

Al-Rikabi, S., M. Bovo, E. Santolini, B. Pulvirenti, A. Barbaresi, D. Torreggiani and P. Tassinari, "Definition of thermal comfort of crops within naturally ventilated greenhouses", Journal of Agricultural Engineering (2023).

Baille, M., A. Baille and J. C. Laury, "Canopy surface resistances to water vapour transfer for nine greenhouse pot plant crops.", Scientia Horticulturae **57**, 143–155, URL `https://agris.fao.org/agris-search/search.do?recordID=NL9402223` (1994).

Bartzanas, T., M. Kacira, H. Zhu, S. Karmakar, E. Tamimi, N. Katsoulas, I. B. Lee and C. Kittas, "Computational fluid dynamics applications to improve crop production systems", Computers and Electronics in Agriculture **93**, 303–313, URL `https://www.sciencedirect.com/science/article/pii/S0168169912001263#!` (2013).

Beckett, K., P. Freer-Smith and G. Taylor, "Particulate pollution capture by urban trees: Effect of species and windspeed", Global Change Biology **6**, 995 – 1003 (2000).

Bekraoui, A., S. Chakir, H. Fatnassi, M. Mouqallid and H. Majdoubi, "Climate behaviour and plant heat activity of a citrus tunnel greenhouse: A computational fluid dynamic study", AgriEngineering **4**, 1095–1115 (2022).

Bitog, J. P., I.-B. Lee, H.-S. Hwang, M.-H. Shin, S.-W. Hong, I.-h. Seo, E. Mostafa and Z. Pang, "A wind tunnel study on aerodynamic porosity and windbreak drag", Forest Science and Technology **7**, 8–16 (2011).

Borges, P., D. França, J. Nazario, C. Monteiro, Z. Mendoza and P. Morais, *Computer program and statistical models to estimate teak leaf area* (2023).

Bouhoun Ali, H., P.-E. Bournet, P. Cannavo and E. Chantoiseau, "Development of a cfd crop submodel for simulating microclimate and transpiration of ornamental plants grown in a greenhouse under water restriction", Computers and Electronics in Agriculture **149**, 26–40 (2018).

Bouhoun Ali, H., P.-E. Bournet, V. Danjou, B. Morille and C. Migeon, "CFD simulations of the night time condensation inside a closed glasshouse: Sensitivity analysis to outside external conditions, heating and glass properties", Biosystems Engineering **127**, 159–175 (2014).

Boulard, T., C. Kittas, J. C. Roy and S. Wang, "Convective and ventilation transfers in greenhouses, part 2: Determination of the distributed greenhouse climate", Biosystems Engineering **83**, 129–147 (2002).

Boulard, T., J.-C. Roy, J.-B. Pouillard, H. Fatnassi and A. Grisey, "Modelling of micrometeorology, canopy transpiration and photosynthesis in a closed greenhouse using computational fluid dynamics.", biosystems engineering **158**, 110–133 (2017).

Boulard, T. and S. Wang, "Experimental and numerical studies on the heterogeneity of crop transpiration in a plastic tunnel", Computers and Electronics in Agriculture **34**, 173–190, URL `https://www.sciencedirect.com/science/article/pii/S0168169901001867` (2002).

Bournet, P.-E. and F. Rojano, "Advances of computational fluid dynamics (cfd) applications in agricultural building modelling: Research, applications and challenges", Computers and Electronics in Agriculture **201**, 107277 (2022).

Buccolieri, R., J. Santiago, E. Rivas and B. Sanchez, "Review on urban tree modelling in cfd simulations: Aerodynamic, deposition and thermal effects", Urban Forestry Urban Greening **31** (2018).

Burger, N., A. Laachachi, M. Ferriol, M. Lutz, V. Toniazzo and D. Ruch, "Review of thermal conductivity in composites: Mechanisms, parameters and theory", Progress in Polymer Science **61** (2016).

Burger, T. A., "A methodology for measuring the wind drag coeeficient on coastal dune vegetation: a study on seaoats (Uniloa paniculata)", SOLAR ENERGY p. 76, URL `https://aquadocs.org/handle/1834/18395` (1992).

Defraeye, T., D. Derome, P. Verboven, J. Carmeliet and B. Nicolaï, "Cross-scale modelling of transpiration from stomata via the leaf boundary layer", Annals of botany **114** (2014).

Dexin, G., Z. Yushu and Z. Tingyao, "A wind-tunnel study of windbreak drag", Agricultural and Forest Meteorology **118**, 75–84 (2003).

Dong, J., J. Peng, X. He, J. Corcoran, S. Qiu and X. Wang, "Heatwave-induced human health risk assessment in megacities based on heat stress-social vulnerability-human exposure framework", Landscape and Urban Planning **203**, 103907 (2020).

Elkins, C. and M. Van Iersel, "Longer photoperiods with the same daily light integral improve growth of rudbeckia seedlings in a greenhouse", HortScience: a publication of the American Society for Horticultural Science **55** (2020).

Endalew, M. A., M. Hertog, M. Delele, K. Baetens, T. Persoons, M. Baelmans, H. Ramon, B. Nicolaï and P. Verboven, "Cfd modelling and wind tunnel validation of airflow through plant canopies using 3d canopy architecture", International Journal of Heat and Fluid Flow **30**, 356–368 (2009).

Fatnassi, H., T. Boulard and L. Bouirden, "Simulation of climatic conditions in full-scale greenhouse fitted with insect-proof screens", Agricultural and Forest Meteorology **118**, 97–111 (2003).

Fatnassi, H., T. Boulard, C. Poncet and M. Chave, "Optimisation of greenhouse insect screening with computational fluid dynamics", Biosystems Engineering **93**, 301–312 (2006).

Fatnassi, H., T. Boulard, J. C. Roy, R. Suay and C. Poncet, "CFD coupled modeling of distributed plant activity and climate in greenhouse.", Acta Horticulturae pp. 57–64 (2017).

Fatnassi, H., C. Poncet, M. M. Bazzano, R. Brun and N. Bertin, "A numerical simulation of the photovoltaic greenhouse microclimate", Solar Energy **120**, 575–584 (2015).

Ghoulem, M., K. El Moueddeb, E. Nehdi, R. Boukhanouf and J. Kaiser Calautit, "Greenhouse design and cooling technologies for sustainable food cultivation in hot climates", Biosystems Engineering **183**, 121–150 (2019).

Gillies, J., W. Nickling and J. King, "Drag coefficient and plant form response to wind speed in three plant species: Burning bush (euonymus alatus), colorado blue spruce (picea pungens glauca.), and fountain grass (pennisetum setaceum)", Journal of Geophysical Research **107**, 4760 (2002).

Gruda, N., M. Bisbis and J. Tanny, "Impacts of protected vegetable cultivation on climate change and adaptation strategies for cleaner production–A review.", Journal of Cleaner Production **225**, 324–339 (2019).

Haxaire, R., *Caractérisation et Modélisation des écoulements d'air dans une serre*, Ph.D. thesis, Université de Nice, Sophia Antipolis (1999).

Hong, B. and B. Lin, "Numerical studies of the outdoor wind environment and thermal comfort at pedestrian level in housing blocks with different building layout patterns and trees arrangement", Renewable Energy **73**, 18–27 (2015).

Kang, G., J.-J. Kim and W. Choi, "Computational fluid dynamics simulation of tree effects on pedestrian wind comfort in an urban area", Sustainable Cities and Society **56**, 102086 (2020).

Kato, S., "Review of airflow and transport analysis in building using cfd and network model", JAPAN ARCHITECTURAL REVIEW **1**, 3, 299–309 (2018).

Kichah, A., P. E. Bournet, C. Migeon and T. Boulard, "Measurement and CFD simulation of microclimate characteristics and transpiration of an Impatiens pot plant crop in a greenhouse", Biosystems Engineering (2012).

Kinyua, D., "A cfd analysis of heat and mass transfer in greenhouses: An introduction", Mathematical Modelling and Applications **2**, 17 (2017).

Koch, K., R. Samson and S. Denys, "Aerodynamic characterisation of green wall vegetation based on plant morphology: An experimental and computational fluid dynamics approach", Biosystems Engineering **178** (2018).

Kumar, M., C. Ojha and J. Saini, "Variability of mass transfer coefficient with roughness elements and approach flow velocity", pp. 2237–2246 (2013).

Launder, B. E. and D. B. Spalding, "The numerical computational of Turbulent flows.", Computer Methods in Applied Mechanics and Engineering **3**, 269–289 (1974).

Lazzaro, L., S. Otto and G. Zanin, "Role of hedgerows in intercepting spray drift: Evaluation and modelling of the effects", Agriculture, Ecosystems Environment **123**, 317–327 (2008).

Li, R., F. Zeng, Y. Zhao, Y. Wu, J. Niu, L. Wang, N. Gao and X. Shi, "Cfd simulations of the tree effect on the outdoor microclimate by coupling the canopy energy balance model", Building and Environment **230**, 109995 (2023).

Limtrakarn, W., P. Boonmongkol, A. Chompupoung, K. Rungprateepthaworn, J. Kruenate and P. Dechaumphai, "Computational fluid dynamics modeling to improve natural flow rate and sweet pepper productivity in greenhouse", Advances in Mechanical Engineering **4**, 158563, URL `https://www.researchgate.net/publication/258381974_Computational_Fluid_Dynamics_Modeling_to_Improve_Natural_Flow_Rate_and_Sweet_Pepper_Productivity_in_Greenhouse` (2012).

Mahjoob Karambasti, B., M. Ghodrat, M. Naghashzadegan and G. Ghorbani, "Optimum design of a greenhouse for efficient use of solar radiation using a multi-objective genetic algorithm", Energy Efficiency **15** (2022).

Majdoubi, H., T. Boulard, H. Fatnassi and L. Bouirden, "Airflow and microclimate patterns in a one-hectare canary type greenhouse: An experimental and cfd assisted study", Agricultural and Forest Meteorology **149**, 1050–1062 (2009).

Manickathan, L., T. Defraeye, J. Allegrini and D. Derome, "Comparative study of flow field and drag coefficient of model and small natural trees in a wind tunnel", Urban Forestry Urban Greening **35** (2018).

Martin, T., G. Fipke, E. Winck and J. Marchese, "Imagej software as an alternative method for estimating leaf area in oats", Acta Agronómica **69** (2021).

Maslak, K., "Thermal energy use in greenhouses the influence of climatic conditions and dehumidification", (2015).

Mochida, A., H. Yoshino, S. Miyauchi and T. Mitamura, "Total analysis of cooling effects of cross-ventilation affected by microclimate around a building", Solar Energy - SOLAR ENERG **80**, 371–382 (2006).

Molina-Aiz, F., F. Domingo, D. L. Valera and A. J. Álvarez, "Measurement and simulation of climate inside Almeria-type greenhouses using computational fluid dynamics", Agricultural and Forest Meteorology **125**, 33–51 (2004).

Molina-Aiz, F., D. Valera, A. Alvarez and A. Madueño, "A wind tunnel study of airflow through horticultural crops: Determination of the drag coefficient", Biosystems Engineering **93**, 447–457 (2006).

Morakinyo, T., K. Dahanayake, O. Adegun and A. Balogun, "Modelling the effect of tree-shading on summer indoor and outdoor thermal condition of two similar buildings in a nigerian university", Energy and Buildings **130**, 721–732 (2016).

Nield, D. and A. Bejan, *Convection in Porous Media*, Springer Science & Business Media (Springer-Verlag, New York, 1999), 2 edn.

Nonomura, T., Y. Matsuda, K. Kakutani, Y. Takikawa, J. Kimbara, K. Osamura, S.-i. Kusakari and H. Toyoda, "Prevention of whitefly entry from a greenhouse entrance by furnishing an airflow-oriented pre-entrance room guarded with electric field screens", Journal of Agricultural Science **6** (2014).

Oke, T. R., "The energetic basis of the urban heat island", Quarterly Journal of the Royal Meteorological Society **108**, 455, 1–24 (1982).

Okushima, L., S. Sase and M. Nara, "A support system for natural ventilation design of greenhouses based on computational aerodynamics", Acta Horticulturae **248**, 129–136 (1989).

Pinard, J. and J. Wilson, "First- and second-order closure models for wind in a plant canopy", Journal of Applied Meteorology **40**, 1762–1768 (2001).

Piscia, D., P. Muñoz, C. Panadès and J. Montero, "A method of coupling cfd and energy balance simulations to study humidity control in unheated greenhouses", Computers and Electronics in Agriculture **115**, 129–141 (2015).

PVGIS, "Photovoltaic geographical information system", URL `http://re.jrc.ec.europa.eu/pvgis/apps3/pvest.php`, accessed on January 10th, 2013 (2020).

Qi, J. and B.-J. He, "Urban heat mitigation strategies", pp. 21–44 (2023).

Ray, A., S. Ghosh and N. Bhowmick, "Solar radiation transmittance characteristics of textile woven fabrics suitable for greenhouse covering materials", Journal of The Institution of Engineers (India): Series E **103** (2021).

Rogers, C., A. Gallant and N. Tapper, "Is the urban heat island exacerbated during heatwaves in southern australian cities?", Theoretical and Applied Climatology **137** (2019).

Roy, J.-C. and T. Boulard, "Cfd prediction of the natural ventilation in a tunnel-type greenhouse: Influence of wind direction and sensibility to turbulence models", Acta Horticulturae **691**, 457–464 (2005).

Roy, J.-C., T. Boulard, C. Kittas and S. Wang, "Pa—precision agriculture: Convective and ventilation transfers in greenhouses, part 1: the greenhouse considered as a perfectly stirred tank", Biosystems Engineering **83**, 1–20 (2002).

Roy, J.-C., C. Vidal, J. Fargues and T. Boulard, "Cfd based determination of temperature and humidity at leaf surface", Computers and Electronics in Agriculture - COMPUT ELECTRON AGRIC **61**, 201–212 (2008).

Saberian, A. and S. M. Sajadiye, "The effect of dynamic solar heat load on the greenhouse microclimate using CFD simulation", Renewable Energy **138**, 722–737 (2019).

Salata, F., I. Golasi, D. Petitti, E. Vollaro, M. Coppi and A. Vollaro, "Relating microclimate, human thermal comfort and health during heat waves: An analysis of heat island mitigation strategies through a case study in an urban outdoor environment", Sustainable Cities and Society **30**, 79–96 (2017).

Santolini, E., B. Pulvirenti, S. Benni, L. Barbaresi, d. Torreggiani and P. Tassinari, "Numerical study of wind-driven natural ventilation in a greenhouse with screens", Computers and Electronics in Agriculture **149**, 41–53 (2018).

Santolini, E., B. Pulvirenti, P. Guidorzi, M. Bovo, D. Torreggiani and P. Tassinari, "Analysis of the effects of shading screens on the microclimate of greenhouses and glass facade buildings", Building and Environment **211**, 108691 (2022).

Santolini, E., B. Pulvirenti, D. Torreggiani and P. Tassinari, "Novel methodologies for the characterization of airflow properties of shading screens by means of wind-tunnel experiments and cfd numerical modeling", Computers and Electronics in Agriculture **163** (2019).

Sase, S., M. Kacira, T. Boulard and O. Limi, "Wind tunnel measurement of aerodynamic properties of a tomato canopy", Transactions of the ASABE **55**, 1921–1927 (2012).

Si, C., F. Qi, X. Ding, F. He, Z. Gao, Q. Feng and L. Zheng, "Cfd analysis of solar greenhouse thermal and humidity environment considering soil–crop–back wall interactions", Energies **16**, 2305 (2023).

Simcenter STAR-CCM+ Academic PowerOn Demand (Siemens 2021).

Stavrakakis, G. M., D. A. Katsaprakakis and K. Braimakis, "A computational fluid dynamics modelling approach for the numerical verification of the bioclimatic design of a public urban area in greece", Sustainability **15**, 15 (2023).

Stewart, I. D., "Redefining the urban heat island", (2011).

Tamimi, E., M. Kacira, C. Y. Choi and L. An, "ANALYSIS OF MICROCLIMATE UNIFORMITY IN A NATURALLY VENTED GREENHOUSE WITH A HIGH-PRESSURE FOGGING SYSTEM", **56**, 3, 1241–1254 (2013).

Teitel, M., S. Ozer and V. Mendelovich, "Airflow temperature and humidity patterns in a screenhouse with a flat insect-proof screen roof and impermeable sloping walls – computational fluid dynamics (cfd) results", Biosystems Engineering **214**, 165–176 (2022).

Thom, A. S., "Momentum absorption by vegetation", Quarterly journal of the Royal Meteorological Society **97(414)**, 414–428 (1971).

Torres, A. and R. Lopez, "Photosynthetic daily light integral during propagation of tecoma stans influences seedling rooting and growth", HortScience **46**, 282–286 (2011).

Tseliou, A., E. Melas, A. Mela, I. Tsiros and E. Zervas, "The effect of green roofs and green façades in the pedestrian thermal comfort of a mediterranean urban residential area", Atmosphere **14**, 1512 (2023).

Upadhyay, K., R. Elangovan and S. Subudhi, "Establishing thermal comfort baseline in a sub-tropical region through a controlled climate chamber study", Advances in Building Energy Research pp. 1–23 (2023).

Wang, S. and T. Boulard, "Measurement and prediction of solar radiation distribution in full-scale greenhouse tunnels", Agronomie **20**, 41–50, URL `https://www.researchgate.net/publication/248848912_Measurement_and_prediction_of_solar_radiation_distribution_in_full-scale_greenhouse_tunnels` (2000).

Yu, G., S. Zhang, S. Li, M. Zhang, H. Benli and Y. Wang, "Numerical investigation for effects of natural light and ventilation on 3d tomato body heat distribution in a venlo greenhouse", Information Processing in Agriculture **10** (2022).

Zhang, Y. and M. Kacira, "Analysis of climate uniformity in indoor plant factory system with computational fluid dynamics (CFD)", Biosystems Engineering **220**, 73–86 (2022).

Zuvela-Aloise, M., R. Koch, S. Buchholz and B. Früh, "Modelling the potential of green and blue infrastructure to reduce urban heat load in the city of vienna", Climatic Change **135**, 425–438 (2016).